Spectroscopy of ^{232}U in the (p, t) reaction: More information on 0^+ excitations

A. I. Levon,[1,*] P. Alexa,[2] G. Graw,[3] R. Hertenberger,[3] S. Pascu,[4] P. G. Thirolf,[3] and H.-F. Wirth[3]

[1]*Institute for Nuclear Research, Academy of Science, Kiev, Ukraine*

[2]*Institute of Physics and Institute of Clean Technologies, Technical University of Ostrava, Czech Republic*

[3]*Fakultät für Physik, Ludwig-Maximilians-Universität München, Garching, Germany*

[4]*H. Hulubei National Institute of Physics and Nuclear Engineering, Bucharest, Romania*

(Received 28 September 2015; published 28 December 2015)

The excitation spectra in the deformed nucleus ^{232}U have been studied by means of the (p,t) reaction, using the Q3D spectrograph facility at the Munich Tandem accelerator. The angular distributions of tritons were measured for 162 excitations seen in the triton spectra up to 3.25 MeV. 0^+ assignments are made for 13 excited states by comparison of experimental angular distributions with the calculated ones using the CHUCK3 code. Assignments up to spin 6^+ are made for other states. Sequences of states are selected which can be treated as rotational bands. Moments of inertia have been derived from these sequences, whose values may be considered as evidence of the two- or one-phonon nature of these 0^+ excitations. Experimental data are compared with interacting boson model and quasiparticle-phonon model calculations.

DOI: 10.1103/PhysRevC.92.064319 PACS number(s): 25.40.Hs, 21.10.Ky, 21.60.−n, 27.90.+b

I. INTRODUCTION

The first observation of multiple excitations with zero angular momentum transfer in the (p,t) reaction seen in the odd nucleus ^{229}Pa [1] initiated an extensive campaign to study 0^+ excitations in even-even actinide nuclei. During the past two decades, many of such investigations have been performed using the Q3D magnetic spectrograph at the Maier-Leibnitz-Laboratory (MLL) Tandem accelerator in Garching, Germany. Because of its very high-energy resolution, this spectrograph is a unique tool in particular for the identification of 0^+ states by measuring the state-selective angular distributions of triton ejectiles. Subsequent analysis is performed within the distorted-wave Born approximation (DWBA). In addition to our studies on the actinide nuclei ^{230}Th, ^{228}Th, ^{232}U, the neighboring odd nucleus ^{229}Pa [2], and most recently on ^{240}Pu [3], the majority of studies on 0^+ excitations was carried out in the regions of rare earth, transitional, and spherical nuclei [4–9]. Most of these studies were limited to measuring the energies and excitation cross sections of 0^+ states. Therefore, they provided only the trend of changes in the nuclei contributing to such excitations in a wide range of deformations: from transitional nuclei (Gd region) to well-deformed (Yb region), γ-soft (Pt region), and spherical nuclei (Pb region). The main result of these studies is the observation of the dependence of the number of 0^+ states as a function of valence nucleon numbers. A particularly large number of low-lying states was interpreted as a signature of a shape phase transition (Gd region), and the sharp drop of the number of low-lying 0^+ states was interpreted as a result of proximity to the shell closure. A particularly interesting result was obtained from the statistical analysis of the distribution of 0^+ energies: Using the Brody distribution function suggests that the spectrum of these excitations is intermediate between ordered and chaotic character. More information from the (p,t) experiments, as well as on the 0^+ excitations in even nuclei, was given in Refs. [6,10,11]. They report data on spins and cross sections for all states observed in the (p,t) reaction. This made it possible to extract information about the moments of inertia for the bands built on the 0^+ states. These experimental studies contributed to the development of theoretical calculations, which explain some of the features of the 0^+ excitation spectra. Some publications have dealt with the microscopic approach [12,13], but the majority of studies used the phenomenological model of interacting bosons (IBM) [14,15]. These approaches have been used also in Ref. [6,10,11]. Nevertheless, the nature of multiple 0^+ excitations in even nuclei is still far from being understood [16].

In this paper, we present the results of a careful and detailed analysis of the experimental data from the high-resolution study of the ^{234}U$(p,t)^{232}$U reaction. A short report on this topic was presented in Ref. [2]. This analysis is similar to the one carried out for the nuclei ^{228}Th and ^{230}Th [10,11]. The nucleus ^{232}U is located in the region of strong quadrupole deformation, where stable reflection-asymmetric octupole deformations occur. Information on excited states of ^{232}U is rather scarce [17]: They have been studied via ^{232}Pa β^- decay, ^{232}Np electron capture decay, ^{236}Pu α decay, and the ^{230}Th$(\alpha,2n\gamma)$ and ^{232}Th$(\alpha,4n\gamma)$ reactions. The study of the (p,t) reaction adds to this information considerably: Data are obtained for 162 levels in the energy range up to 3.25 MeV. Besides 0^+ states, where the number of reliable assignments could be increased from 9 to 13 states in comparison to the preliminary analysis in Ref. [2], information on the spins up to 6^+ for many other states was obtained. Some levels are grouped into rotational bands, thus allowing to derive the moment of inertia for some 0^+, 2^+ and 0^-, 1^-, 2^-, 3^- bands.

II. EXPERIMENT DETAILS AND RESULTS

A. Details of the experiment

The (p,t) experiment has been performed at the Tandem accelerator of the Maier-Leibnitz-Laboratory of the

*levon@kinr.kiev.ua

Ludwig-Maximilians-Universität and Technische Universität München. A radioactive target of 100 μg/cm^2 ^{234}U with half-life $T_{1/2} = 2.45 \times 10^5$ yr, evaporated on a 22 μg/cm^2 thick carbon backing, was bombarded with 25-MeV protons at an intensity of 1–2 μA on the target. The isotopic purity of the target was about 99%. The reaction products have been analyzed with the Q3D magnetic spectrograph and then detected in a focal plane detector. The focal plane detector is a multiwire proportional chamber with readout of a cathode foil structure for position determination and dE/E particle identification [18,19]. The acceptance of the spectrograph was 11 msr, except for the most forward angle of 5° with an acceptance of 6 msr. The resulting triton spectra have a resolution of 4–7 keV (full width at half maximum) and are background free. The experimental runs were normalized to the integrated beam current measured in a Faraday cup behind the target. The angular distributions of the cross sections were obtained from the triton spectra at 12 different laboratory angles from 5° to 50° in two sets: the first one with higher accuracy for energies up to 2350 keV and the second one with somewhat lower accuracy for energies from 2200 to 3250 keV.

A triton energy spectrum measured at a detection angle of 5° is shown in Fig. 1. At this angle, the 0^+ states have comparatively large cross sections. The analysis of the triton spectra was performed using the program GASPAN [20]. For the calibration of the energy scale, the triton spectra from the reactions ^{184}W$(p,t)^{182}$W and ^{186}W$(p,t)^{184}$W were measured at the same magnetic settings. The known levels in ^{232}U [17] and the levels in ^{228}Th known from the study [11] were also included in the calibration.

The peaks in the energy spectra for all 12 angles were identified for 162 levels. The information obtained for these levels is summarized in Table I. The energies and spins of the levels as derived from this study are compared to known

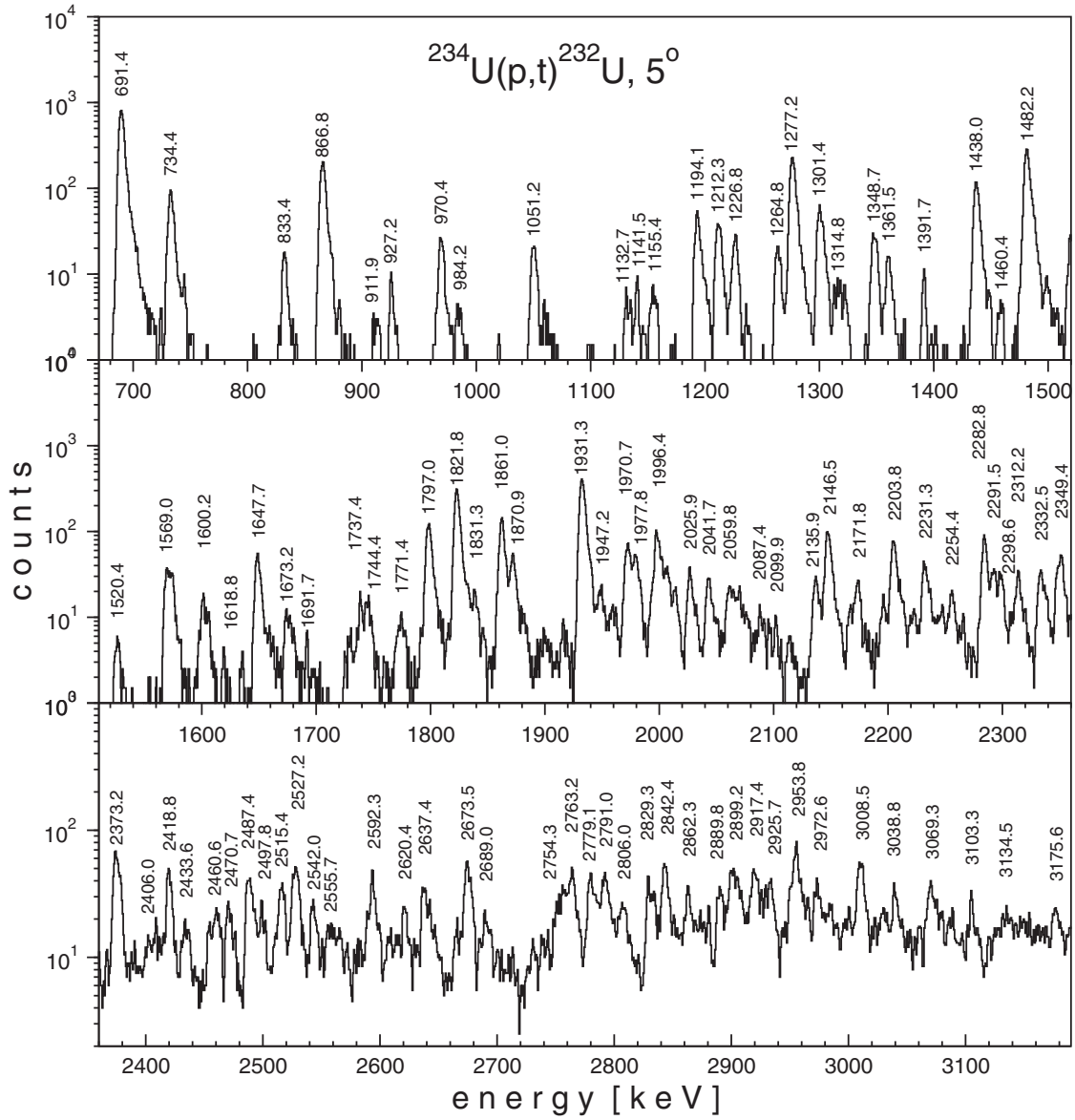

FIG. 1. Triton energy spectrum from the ^{234}U$(p,t)^{232}$U reaction ($E_p = 25$ MeV) in logarithmic scale for a detection angle of 5°. Some strong lines are labeled with their corresponding level energies in keV.

TABLE I. Energies of levels in ^{232}U, the level spin assignments from the CHUCK3 analysis, the (p,t) cross sections integrated over the measured values (i.e., 5° to 50°) and the reference to the schemes used in the DWBA calculations (see text for more detailed explanations).

Level energy (keV)		I^π			Ratio	Way of
This work	NDS [17]	This work	NDS [17]	$\sigma_{\text{integ.}}$ (μb)	$\sigma_{\text{exp.}}/\sigma_{\text{calc.}}$	fitting
0.0 *1*	0.00	0^+	0^+	183.90 *58*	8.95	sw.gg
47.6 *1*	47.573(8)	2^+	2^+	43.40 *35*	50.5	m1a.gg
156.6 *1*	156.566(9)	4^+	4^+	8.11 *35*	1.20	m1a.gi
322.6 *2*	322.69(7)	6^+	6^+	5.55 *40*	178	m2d.gg
541.1 *4*	541.1(1)	(8^+)	8^+	0.42 *20*	0.75	m2c.gg
563.2 *4*	563.194(7)	1^-	1^-	0.90 *25*	0.12	m1a.gg
628.8 *4*	628.965(8)	3^-	3^-	2.70 *33*	0.24	m3a.gg
691.4 *2*	691.42(9)	0^+	0^+	35.00 *70*	194	sw.ii
734.4 *2*	734.57(5)	2^+	2^+	21.68 *65*	2.85	m1a.gi
746.5 *5*	746.8(1)		(5^-)	0.35 *18*		
833.4 *2*	833.07(20)	4^+	4^+	3.21 *23*	0.55	m1a.gg
866.8 *2*	866.790(8)	2^+	2^+	64.05 *90*	8.15	m1a.gi
911.9 *4*	911.49(4)	3^+	(3^+)	1.08 *15*	6.75	m2a.gg
914.5 *9*	915.2(4)		7^-	0.10 *06*		
927.2 *4*	927.3(1)	$0^+ + 2^+$	(0^+)	0.35 *10*	1.45	sw.ii
967.1 *9*	967.6(1)		(2^+)	0.65 *35*		
970.4 *3*	970.71(7)	4^+	(4^+)	4.65 *32*	69.0	m1a.ij
984.2 *9*	984.9(2)	6^+	6^+	0.40 *12*	13.0	m2d.gg
1015.9 *9*	1016.850(8)	(2^-)	2^-	0.12 *07*	0.20	m2f.gg
1051.2 *3*	1050.90(1)	3^-	3^-	3.45 *25*	0.24	m1a.gg
1060.8 *8*		(3^-)		0.32 *12*	0.14	m2a.gg
1097.6 *8*	1098.2(4)	(4^-)	(4^-)	0.10 *06*	3.15	m2a.gg
1132.7 *3*	1132.97(10)	2^+	(2^+)	1.52 *18*	0.15	sw.gg
1141.5 *4*		(1^-)		1.02 *15*	0.13	m1a.gg
1155.4 *4*		5^-		1.38 *35*	0.78	m2e.gg
		or 3^+			6.40	m2a.gg
1173.0 *6*	1173.06(17)	2^-	$(2)^-$	0.52 *12*	6.12	m2a.gg
1194.1 *3*	1194.0(2)	4^+	$(3+,4^+)$	3.18 *53*	1.65	m2a.gg
1212.3 *3*	1211.3(3)	3^-	3^-	6.60 *55*	0.46	m1a.gg
1226.8 *4*		4^+		2.64 *26*	0.33	m1a.gj
1264.8 *3*		3^-		2.42 *22*	1.00	m2a.gg
1277.2 *3*		0^+		16.12 *60*	0.45	sw.gg
1301.4 *3*		2^+		3.00 *25*	3.95	m1a.gg
1314.8 *4*		6^+		3.57 *28*	13.3	m2e.gg
1321.8 *5*		2^+		0.57 *20*	2.90	sw.jj
		or 3^-			0.12	m3a.gg
1348.7 *3*		(2^+)		3.25 *25*	14.5	sw.jj
1361.5 *4*		4^+		1.00 *16*	0.45	m2a.gg
		or 3^-			0.16	m3a.gg
1372.0 *6*		2^+		0.30 *12*	0.03	m1a.ig
		or 6^+			0.33	m2d.gg
1391.7 *4*		4^+		0.85 *15*	0.12	m1a.gg
		or 5^-			12.0	sw.ji
1438.0 *3*		4^+		12.72 *55*	205.	m1a.ij
1460.4 *6*		6^+		0.85 *15*	0.27	m2d.gg
1482.2 *3*		0^+		14.15 *55*	27.25	sw.ig
1489.2 *4*		2^+		4.18 *50*	0.45	sw.gg
1501.4 *7*		3^-		0.68 *15*	41.8	sw.jj
1520.4 *4*		2^+		6.85 *33*	150.	m1a.ii
1552.8 *8*		(3^+)		0.83 *15*	4.60	m2a.gg
1569.0 *4*		0^+		3.72 *36*	8.15	sw.ig
1572.9 *6*		4^+		3.45 *36*	31.5	sw.jj
1600.2 *6*		2^+		1.40 *25*	1.50	m1a.gg
1605.4 *8*		4^+		0.72 *22*	6.15	m1a.ij
1618.8 *7*		2^+		0.62 *15*	0.08	m1a.ig

TABLE I. (*Continued.*)

Level energy (keV)		I^π			Ratio	Way of
This work	NDS [17]	This work	NDS [17]	$\sigma_{\text{integ.}}$ (μb)	$\sigma_{\text{exp.}}/\sigma_{\text{calc.}}$	fitting
1633.8 *6*		3^+		1.35 *25*	5.05	m2a.gg
		or 6^+			16.0	sw.jj
1647.7 *5*		2^+		24.88 *50*	3.15	m1a.gg
1673.2 *5*		4^+		1.72 *25*	0.35	sw.gg
1679.8 *6*		1^-		1.25 *22*	0.04	m1a.gg
		or 3^-			0.06	m3a.gg
1691.7 *6*		(6^+)		1.05 *18*	4.20	m2e.gg
1700.5 *8*		6^+		0.85 *18*	0.20	sw.gg
1728.5 *6*		(4^+)		1.08 *22*	0.20	m1a.gg
1737.4 *5*		(6^+)		3.25 *33*	0.35	m3a.gg
1744.4 *5*		4^+		4.86 *40*	0.85	m1a.gg
		or 5^-			2.70	m2e.gg
1758.9 *9*		(5^-)		0.69 *15*	19.0	sw.ii
1771.4 *8*				2.96 *26*		
1790.8 *7*		6^+		2.05 *28*	7.50	m2e.gg
1797.0 *5*		0^+		10.15 *65*	11.0	sw.ii
1802.5 *9*		(4^+)		0.88 *45*	9.80	sw.ij
1821.8 *5*		0^+		20.65 *70*	27.2	sw.ii
1831.7 *5*		(2^+)		1.38 *30*	0.22	m1a.gg
1838.6 *6*		2^+		1.16 *26*	1.40	m1a.gg
1861.0 *5*		0^+		9.63 *50*	11.2	sw.ig
1870.9 *5*		2^+		14.18 *65*	1.70	m1a.gi
1880.8 *5*		6^+		2.08 *35*	0.18	m3a.gg
1900.0 *6*				1.25 *25*		
1915.2 *8*		6^+		1.85 *30*	7.40	m2d.gg
1931.3 *5*		0^+		29.55 *75*	140	sw.ig
1947.2 *8*		(0^+)		1.52 *30*	7.60	sw.ig
1957.4 *8*		6^+		3.05 *35*	11.9	m2d.gg
1970.7 *5*		2^+		25.65 *95*	2.70	sw.ig
1977.8 *5*		2^+		20.05 *90*	2.25	m1a.gg
1996.4 *5*		4^+		15.20 *65*	108	sw.ij
2004.9 *6*		4^+		4.70 *50*	46.0	sw.ij
2011.6 *6*				2.30 *65*		
2025.9 *6*		0^+		2.96 *35*	19.0	sw.ii
2041.7 *5*		2^+		10.85 *55*	1.20	m1a.gg
2059.8 *5*		2^+		10.65 *55*	1.20	m1a.gg
2068.6 *5*		4^+		3.40 *45*	0.42	sw.gg
2073.4 *9*				1.30 *40*		
2087.4 *6*		5^-			1.95	m2e.gg
		or 6^+			53.0	sw.jj
2094.2 *8*				1.20 *40*		
2099.9 *6*		6^+		1.62 *35*	21.3	sw.jj
2135.9 *5*		4^+		4.22 *55*	32.4	m1a.ij
2146.5 *5*		2^+		39.80 *98*	4.60	m1a.gg
2171.8 *5*		2^+		8.81 *55*	1.00	sw.gg
2194.6 *5*		2^+		4.08 *55*	0.45	sw.gg
2203.8 *5*		2^+		29.20 *95*	3.15	sw.gg
2221.3 *9*				1.22 *45*		
2231.3 *5*		4^+		10.38 *58*	67.0	m1a.ij
2235.9 *5*				2.00 *60*		
2246.2 *5*				1.55 *55*		
2254.4 *5*		6^+		5.35 *45*	19.2	m2d.gg
2282.8 *5*		2^+		29.30 *70*	3.30	m1a.gg
2291.5 *5*		2^+		11.23 *90*	1.28	m1a.gg
2298.6 *5*		2^+		4.73 *85*	1.35	sw.gg
2312.2 *6*		4^+		3.95 *75*	28.5	m1a.ij

TABLE I. (*Continued.*)

Level energy (keV)		I^π			Ratio	Way of
This work	NDS [17]	This work	NDS [17]	$\sigma_{\text{integ.}}$ (μb)	$\sigma_{\text{exp.}}/\sigma_{\text{calc.}}$	fitting
2332.5 *6*		2^+		8.98 *65*	1.10	m1a.gg
2349.4 *6*		2^+		17.27 *86*	2.05	m1a.gg
2373.2 *6*		2^+		19.15 *90*	2.25	m1a.gg
2397.7 *6*		2^+		2.48 *48*	0.21	sw.gg
2406.0 *6*		6^+		2.80 *68*	12.8	m2e.gg
		or 5^-			110	sw.ij
2412.4 *6*		2^+		3.67 *90*	0.35	m1a.gg
2418.8 *5*		2^+		11.88 *92*	1.45	m1a.gg
2433.6 *5*		3^-		2.61 *47*	3.80	m2a.gg
2454.2 *5*		(3^-)		1.67 *96*	2.60	m2a.gg
2460.6 *5*		3^-		4.14 *98*	5.20	m2a.gg
		or 6^+			0.45	m3a.gg
2470.7 *6*		(3^-)		3.32 *63*	4.90	m2a.gg
2487.4 *5*		3^-		5.96 *68*	8.90	sw.gg
2497.8 *6*		(4^+)		2.82 *58*	21.4	m1a.ij
2515.4 *6*		(3^-)		8.21 *74*	10.8	m2a.gg
2527.2 *6*		4^+		7.69 *73*	46.0	m1a.ij
2542.0 *7*		2^+		5.88 *69*	0.67	m1a.gg
2555.7 *8*		(4^+)		1.98 *62*	11.2	m1a.ij
2564.7 *8*		(3^-)		1.82 *62*	2.60	m2a.gg
2582.9 *8*				1.85 *66*		
2592.3 *7*		4^+		5.78 *71*	32.9	m1a.ij
2598.7 *9*				1.20 *40*		
2608.0 *9*		2^+		2.15 *53*	0.32	m1a.gg
2620.4 *6*				2.75 *62*		
2637.4 *6*		6^+		6.84 *87*	0.65	m3a.gg
		or 5^-			180	sw.ij
2642.0 *7*				1.78 *80*		
2664.6 *7*		4^+		1.75 *45*	11.5	m1a.ij
2673.5 *7*		2^+		9.11 *76*	1.08	m1a.gg
2689.0 *8*		2^+		3.45 *58*	0.38	m1a.gg
2754.3 *7*		4^+		4.89 *68*	29.5	m1a.ij
2763.2 *6*		(3^-)		6.08 *70*	8.95	sw.gg
2779.1 *6*		2^+		7.21 *70*	0.92	m1a.gg
2791.0 *7*		2^+		8.90 *75*	1.18	m1a.gg
2806.0 *7*		2^+		4.50 *62*	0.66	m1a.gg
2829.3 *7*		4^+		5.98 *65*	34.5	m1a.ij
2842.4 *7*		4^+		7.12 *75*	38.0	m1a.ij
2850.6 *7*		6^+		2.63 *63*	11.9	m2d.gg
2862.3 *7*		3^-		4.58 *63*	6.75	sw.gg
2878.3 *7*		(6^+)		4.45 *63*	345	sw.ig
2889.8 *6*		4^+		4.60 *72*	26.0	m1a.ij
2899.2 *7*		(4^+)		5.1 *15*	0.75	sw.gg
2905.8 *7*				3.5 *16*		
2917.4 *7*		0^+		5.58 *92*	8.95	sw.ji
2925.7 *8*		(6^+)		3.4 *18*	14.5	m2d.gg
2931.5 *7*		(5^-)		5.8 *20*	61.0	sw.ij
2953.5 *8*		4^+		9.60 *80*	58.5	m1a.ij
2959.7 *7*		(2^+)		3.05 *60*	8.90	sw.ig
2972.6 *8*		2^+		4.70 *65*	0.48	m1a.gg
2984.2 *8*				1.09 *50*		
2998.7 *8*		(2^+)		2.40 *54*	7.40	sw.ig
3008.5 *8*		(3^-)		2.80 *65*	0.52	m3a.gg
3028.8 *8*		4^+		2.05 *55*	12.0	m1a.ij
3038.8 *8*		(5^-)		4.40 *63*	145	sw.ij
3058.3 *9*		(6^+)		1.00 *50*	91.0	sw.ig

TABLE I. (*Continued.*)

Level energy (keV)		I^π			Ratio	Way of
This work	NDS [17]	This work	NDS [17]	$\sigma_{\text{integ.}}$ (μb)	$\sigma_{\text{exp.}}/\sigma_{\text{calc.}}$	fitting
3069.3 *8*		3^-		5.04 *75*	6.75	m2a.gg
3075.7 *9*		(5^-)		1.88 *65*	61.5	sw.ij
3087.5 *9*		2^+		1.70 *65*	0.20	m1a.gg
3103.3 *9*		(4^+)		1.95 *55*	10.2	m1a.ij
3134.5 *9*		(4^+)		1.68 *55*	9.90	m1a.ij
3149.1 *9*		2^+		1.85 *55*	41.8	sw.ij
		or 3^-			2.60	m2a.gg
3175.6 *8*		(2^+)		1.96 *55*	42.0	sw.ij

energies and spins from Ref. [17]. They are given in the first four columns. The column labeled $\sigma_{\text{integ.}}$ gives the cross section integrated in the region from 5° to 50°. The column entitled $\sigma_{\text{exp.}}/\sigma_{\text{calc.}}$ gives the ratio of the integrated cross sections, obtained from experimental values, from calculations in the DWBA approximation (see Sec. II B). The last column lists the notations of the schemes used in the DWBA calculations: sw.jj means one-step direct transfer of the $(j)^2$ neutrons in the (p,t) reaction; notations of the multistep transfers used in the DWBA calculations are displayed in Fig. 2.

B. DWBA analysis

We assume that a *(lj)* pair transferred in the (p,t) reaction is coupled to spin zero, and that the overall shape of the angular distribution of the cross section is rather independent of the specific structure of the individual states, because the wave function of the outgoing tritons is restricted to the nuclear exterior and therefore to the tails of the triton form factors. At the same time, cross sections for different orbits have to differ strongly in magnitude. To verify this assumption, DWBA calculations of angular distributions for different $(j)^2$ transfer configurations to states with different spins were carried out in our previous paper [10]. Indeed, the magnitude of the cross sections differs strongly for different orbits, but the shapes of calculated angular distributions are very similar. Nevertheless, they depend to some degree on the transfer configuration, the most pronounced being found for the 0^+ states, which is confirmed by the experimental

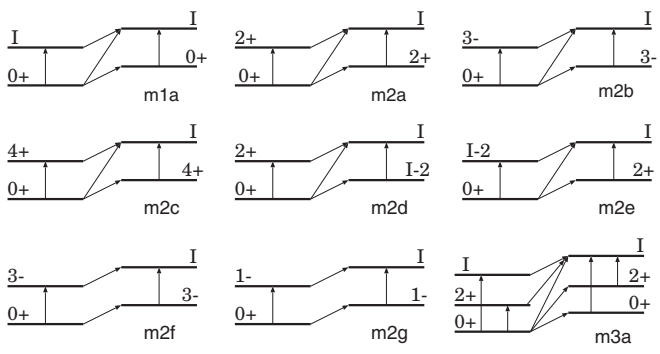

FIG. 2. Schemes of the CHUCK3 multistep calculations tested with spin assignments of excited states in ^{232}U (see Table I).

angular distributions. This is true for most of the *(lj)* pairs and only for the case of a one-step transfer. No complication of the angular distributions is expected for the excitation of 0^+ states, which proceeds predominantly via a one-step process. This is not the case for the excitation of states with other spins, where the angular distribution may be altered owing to inelastic scattering (coupled-channel effect), treated here as multistep processes. Taking into account these circumstances allows for a reliable assignment of spins for most of the excited states in the final nucleus ^{232}U by fitting the angular distributions obtained in the DWBA calculations to the experimental ones. The assignment of a single spin has not been possible only in a few cases, for which two or even three spin values are allowed.

The magnitude and shape of the DWBA cross section angular distributions depends on the chosen potential parameters. We used the optical potential parameters suggested by Becchetti and Greenlees [21] for protons and by Flynn *et al.* [22] for tritons. These parameters have been tested via their description of angular distributions for the g.s. of ^{228}Th, ^{230}Th, and ^{232}U [2]. Minor changes of the parameters for tritons were needed only for some 3^- states, particularly for the states at 628.8, 1051.2, and 1212.3 keV. For these states, the triton potential parameters suggested by Becchetti and Greenlees [23] have been used. For each state the binding energies of the two neutrons are calculated to match the outgoing triton energies. The corrections to the reaction energy are introduced depending on the excitation energy. For more details, see Ref. [10].

The coupled-channel approximation (CHUCK3 code of Kunz [24]) was used in previous [10,11] and present calculations. The best reproduction of the angular distribution for the ground state and for the 1277.2-keV state was obtained for the transfer of the $(2g_{9/2})^2$ configuration in the one-step process. This orbital is close to the Fermi surface and was considered in previous studies [10,11] as the most probable one in the transfer process. However, for ^{232}U, a better reproduction of the angular distributions for other 0^+ states is obtained for the configuration $(1i_{11/2})^2$, also near the Fermi surface, alone or in combination with the $(2g_{9/2})^2$ configuration. The only exception is the state at 2917.4 keV, for which the experimental angular distribution can be fitted only by the calculated one for the transfer of the $(1j_{15/2})^2$ neutron configuration.

Results of fitting the angular distributions for the states assigned as 0^+ excitations are shown in Fig. 3. The agreement

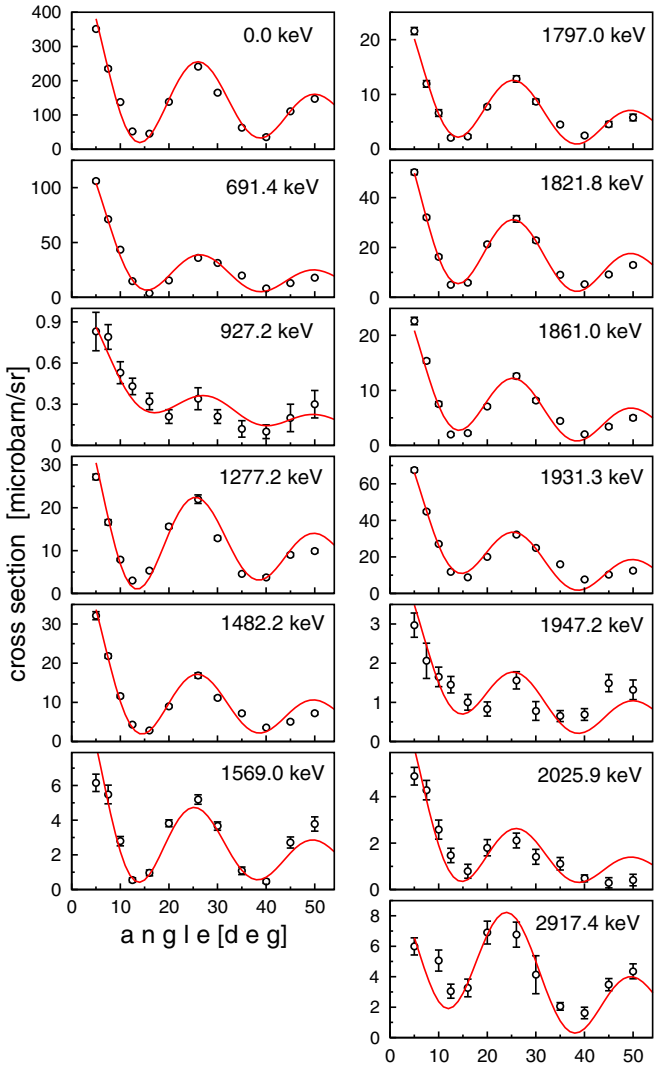

FIG. 3. (Color online) Angular distributions of assigned 0^+ states in ^{232}U and their fit with CHUCK3 one-step calculations. The transfer configurations used in the calculations for the best fit are given in Table I. See text for further information.

between the fit and the data is excellent for most of the levels. Remarks are needed only for the level at 927.2 keV. The existence of this state and the state at the energy of 967.7 keV was established by the γ energies and the coincident results at the α decay of ^{236}Pu [25]. Strong evidence has been obtained that these states have spins 0^+ and 2^+ and are the members of a $K^\pi = 0^+$ band. At the same time, it was noted that the occurrence of a 927.7-keV γ ray is in contradiction with the 0^+ assignment for this state if this γ ray corresponds to a ground-state transition from the 927.7-keV state. Alternatively, this transition should be placed in another location. The measured (p,t) angular distribution for the 927.7-keV state strongly peaks in the forward direction, which is typical for the $L = 0$ transfer but the lack of a deep minimum at about 14° contradicts the 0^+ assignment. The assumption that a doublet with spins 0^+ and 2^+ occurs at the energy of 927.7 keV seems to be a unique explanation of the experimental data. The angular distribution in this case is fitted by the calculated one satisfactorily, as one can see in Fig. 3. To obtain a satisfactory fit, one has to assume a population of the 2^+ state at about 1/3 of the population of the 0^+ state. Thus, we can make firm 0^+ assignments for 12 states for energy excitations below 3.25 MeV, in comparison with 9 states found in the preliminary analysis of the experimental data [2]. The assignment for the 1947.2-keV level is tentative. We can compare 24 0^+ states in ^{230}Th and 18 0^+ states in ^{228}Th with only 13 0^+ states in ^{232}U in the same energy region.

The main goal of many studies using two-neutron transfer in the regions of rare-earth, transitional, and spherical nuclei [4–9] was to collect information only about the 0^+ states, their energies, and excitation cross sections. At the same time the states with nonzero spin are intensively excited in the (p,t) reaction and information about them can be obtained from the analysis of the angular distributions. The main features of the angular distribution shapes for 2^+, 4^+, and 6^+ states are even more weakly dependent on the transfer configurations only in the case of one-step transfer. Therefore, the $(2g_{9/2})^2$, $(1i_{11/2})^2$, and $(1j_{15/2})^2$ configurations, alone or in combination, were used in the calculations for these states. The one-step transfer calculations give a satisfactory fit of angular distributions for about 30% of the states with spins different from 0^+ and the inclusion of multistep excitations for about 70% of the states is needed. As in the Th isotopes [10,11], multistep excitations have to be included to fit the angular distributions already for the 2^+, 4^+, and 6^+ states of the ground-state (g.s.) band. At least a small admixture of multistep transfer for most of the other states is required to get a good agreement with experiment. Figure 2 shows the schemes of the multistep excitations, tested for every state in those cases, where one-step transfer did not provide a successful fit. Figure 4 demonstrates the quality of the fit of different-shaped angular distributions at the excitation of states with spin 2^+ by calculations assuming one-step and one-step plus two-step excitations. Results of similar fits for the states assigned as 4^+, 6^+ and 1^-, 3^-, 5^- excitations are shown in Fig. 5. At the same time, for a number of states, possibly owing to a lack of statistical accuracy, a good fit of the calculated angular distributions to the experimental ones cannot be achieved for a unique spin of the final state and therefore uncertainties remain in the spin assignment for such states. Some of them are demonstrated in Fig. 6.

The spins and parities resulting from such fits are presented in Table I, together with other experimental data. Figure 7 summarizes the (p,t) strengths integrated over the angle region 5°–50° for positive-parity states. The sixth column in Table I displays the ratio $\sigma_{\text{exp.}}/\sigma_{\text{calc.}}$. Calculated cross sections for the specific transfer configurations differ very strongly. If the microscopic structure of the excited states is known, and thus the relative contribution of the specific $(j)^2$ transfer configurations to each of these states, these relationships are considered as spectroscopic factors. A perfect fit of the experimental angular distributions may mean that the assumed configurations in the calculations correspond to the major components of the real configurations. Therefore, at least the order of magnitude for the ratio $\sigma_{\text{exp.}}/\sigma_{\text{calc.}}$ corresponds to the actual spectroscopic factors with the exception of too large values, such as in the case of the $(1i_{11/2})^2$ transfer

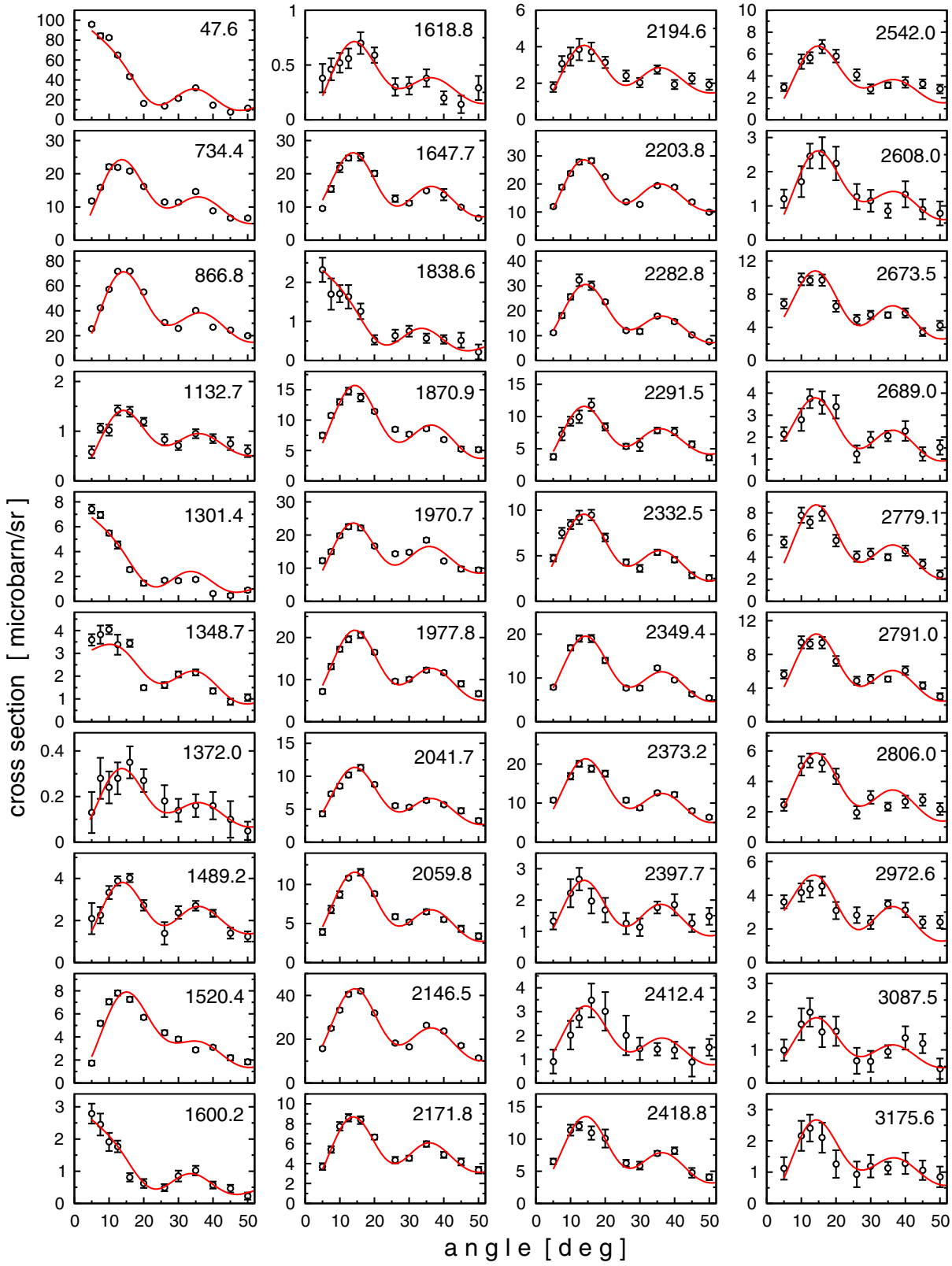

FIG. 4. (Color online) Angular distributions of assigned 2^+ states in ^{232}U and their fit with CHUCK3 calculations. The (ij) transfer configurations and schemes used in the calculations for the best fit are given in Table I.

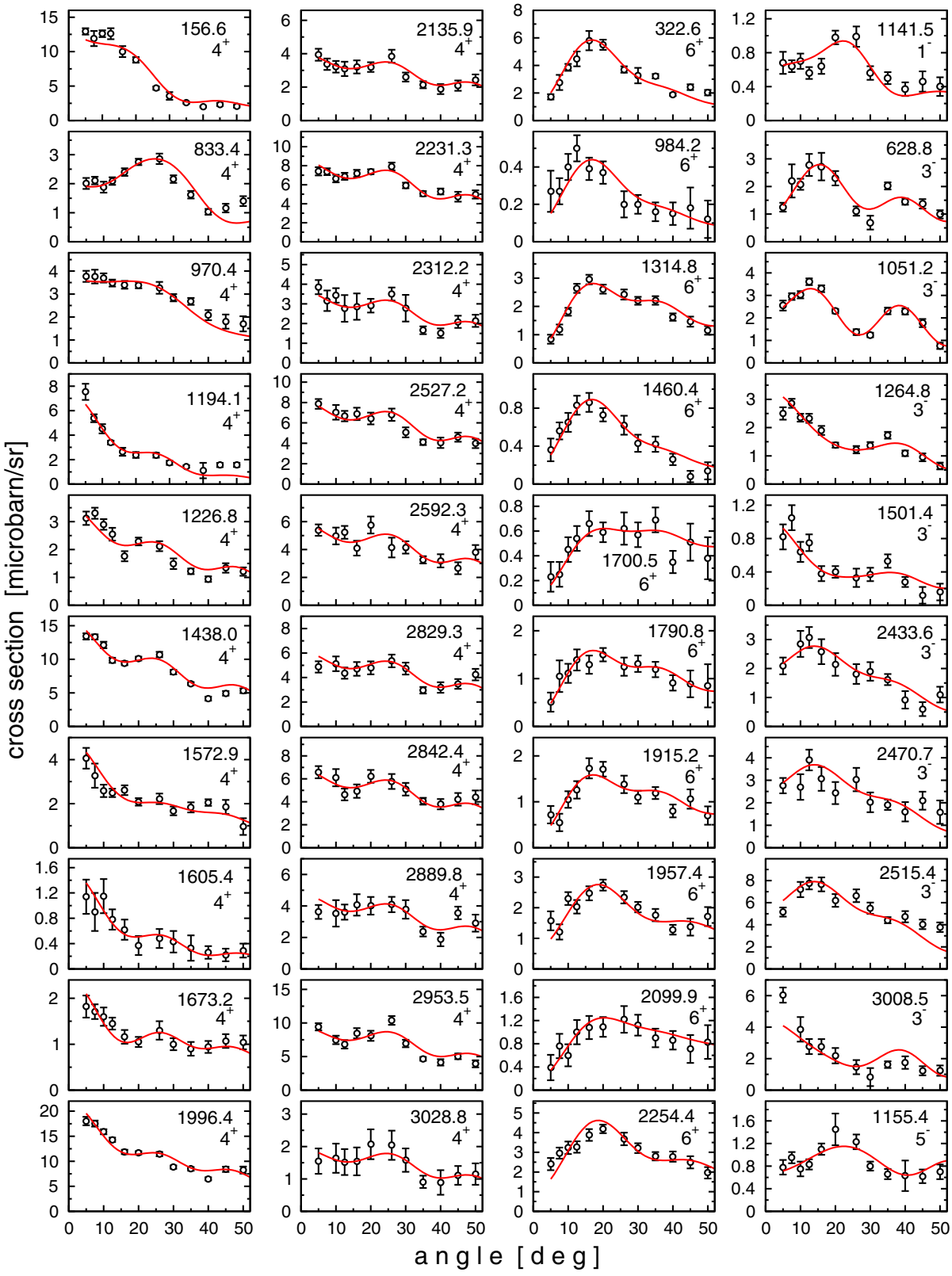

FIG. 5. (Color online) Angular distributions of some assigned states in ^{232}U and their fit with CHUCK3 calculations: 4^+ and 6^+ with positive parity and 1^-, 3^-, and 5^- with negative parity. The (ij) transfer configurations and schemes used in the calculations for the best fit are given in Table I.

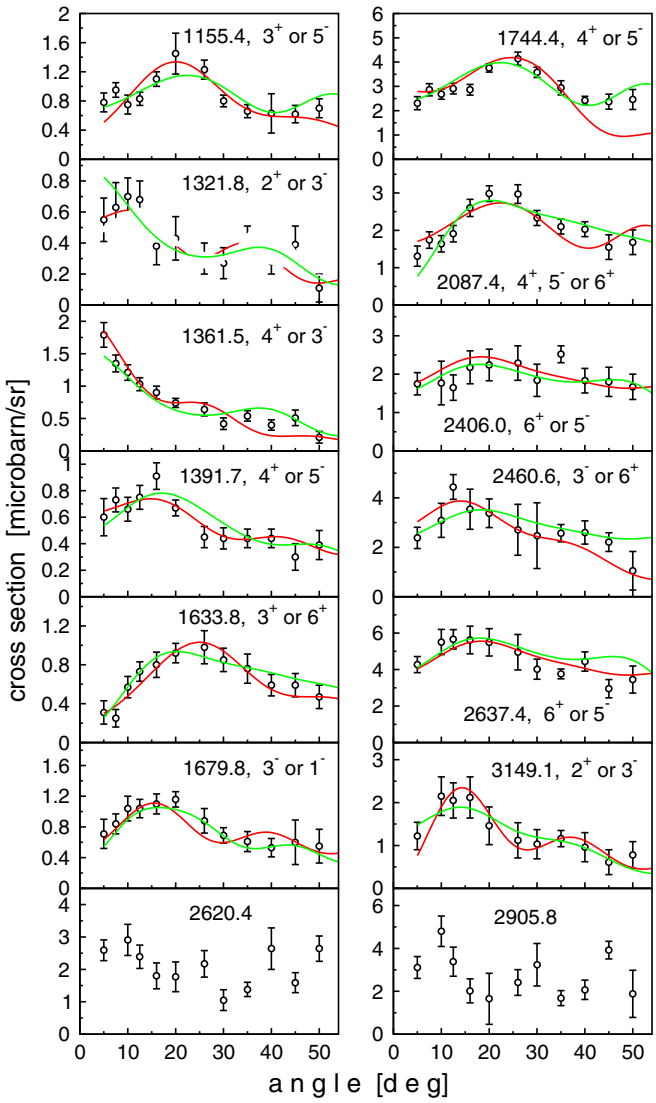

FIG. 6. (Color online) Angular distributions for some states in ^{232}U for which fitting of the calculated distributions for a unique spin is doubtful or not possible. The first spin is indicated by red color.

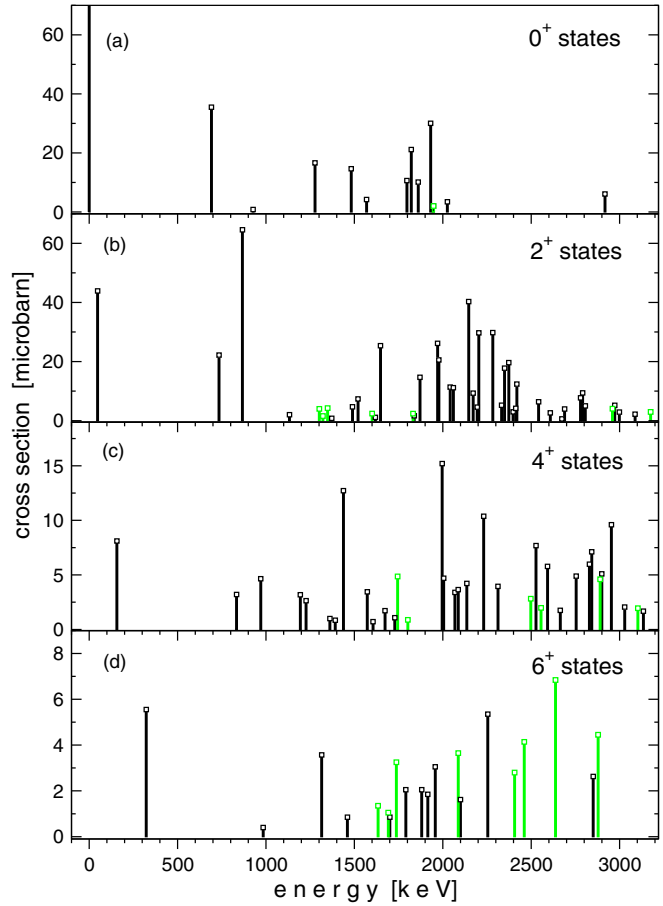

FIG. 7. (Color online) Experimental distribution of the (p,t) strength integrated in the angle region 5°–50° for 0^+, 2^+, 4^+, and 6^+ states in ^{232}U. Green lines represent tentative assignments.

configurations used in the calculation for some 0^+ and even 2^+ and 4^+ states. Surprisingly, the shape just for this neutron configuration gives the best agreement with experiment for the mentioned states.

A few additional comments have to be added for the region where data about the spins and parities are known from the analysis of γ spectra [17]. The angular distributions for some states are very different from those calculated for the one-step transfer. Therefore, they were used as examples for other states at higher energies in the analysis of the angular distributions. As already noted, the difference is significant already for the 2^+ and 4^+ states of the g.s. band. For example, the angular distribution for the 2^+ state at 47.6 keV can be used as a example for the states at 1301.4, 1600.2, and 1838.6 keV. From the two spins 3^+ and 4^+ proposed for the state at 1194.1 keV in the analysis of the γ spectra [17], our data clearly confirm the spin 4^+. Then the angular distribution for this state can serve as an example for the states at 1361.5 and 1604.9 keV. Importantly, the angular distributions for some 2^+ and 4^+ states have a feature typical for the excitation of 0^+ states, namely a strong peak at small angles.

The angular distribution for the 4^+ state at 833.4 keV, which is known from the γ spectroscopy, is very different from the one for the one-step transfer. It was used as an example for the assignment of spins of the states at 1728.5 and 1744.4 keV with similar angular distributions. Similarly, the angular distribution for the 1^- state at 563.2 keV can serve as an example for the state at 1141.3 keV. The angular distribution for the state 3^- at 628.8 keV not only differs from the one calculated for one-step transfer and can be described by the scheme m3a.gg, but it is very similar to the angular distribution for the 2^+ state at one-step transfer. Therefore, for all states with similar experimental distributions, the calculated angular distributions for the spins 2^+ and 3^- were tested during a fitting procedure, using the scheme m3a.gg.

The states with unnatural parity populated via two-neutron transfer, such as 3^+ at 911.9 keV and 2^- at 1173.0 keV, represent a special case. Assignments based on the γ-spectra analysis are tentative. As one can see from Fig. 6, these spins and parities are confirmed by fitting the angular distributions. Spin 3^+ for the states at 1552.8 and 1633.8 keV

is attributed taking into account also the similarity of their angular distributions with those for the state at 911.9 keV. The state at 1015.9 keV is excited weakly, but the angular distribution measured with small statistics does not contradict the assignment of spin 2^-. The same is true for the state at 1097.6 keV with spin 4^-.

III. DISCUSSION

A. Collective bands and moments of inertia in ^{232}U

Aiming to get more information on the excited states in ^{232}U, especially on the moments of inertia for the 0^+ states, we have attempted to identify those sequences of states, which show the characteristics of a rotational band structure. An identification of the states attributed to rotational bands can be made on the basis of the following conditions: (a) the angular distribution for a band member candidate is fitted by DWBA calculations for its expected spin; (b) the transfer cross section in the (p,t) reaction to states in the potential band has to decrease with increasing spin; (c) the energies of the states in the band can be fitted approximately by the expression for a rotational band $E = E_0 + AI(I+1)$ with a small and smooth variation of the inertial parameter A. Collective bands identified in such a way are listed in Table II. The procedure can be justified, because some sequences meeting the above criteria are already known to be rotational bands from γ-ray spectroscopy [17]. In Fig. 8 we present moments of inertia (MoI) obtained by fitting the level energies of the bands displayed in Table II by the expression $E = E_0 + AI(I+1)$ for close-lying levels; i.e., they were determined for band members using the ratio of ΔE and $\Delta[I(I+1)]$, thus saving the spin dependence of the MoI.

Negative-parity states. Unlike the thorium isotopes [10,11], some uncertainties in the formation of the bands are met for ^{232}U. At the beginning a few comments follow about the lowest negative-parity states, usually interpreted as of octupolar vibrational character. They are one-phonon octupole excitations, forming a quadruplet of states with $K^\pi = 0^-,1^-,2^-,3^-$ and are the bandheads for the rotational bands. The $K^\pi = 0^-$ band is reliably established [17] and confirmed by the present study. There are two states with $J^\pi = 2^-$ at 1016.8 and 1173.1 keV, which may be members of bands with $K^\pi = 1^-$ and $K^\pi = 2^-$. The level at 1146.3 keV has been proposed as a bandhead of the $K^\pi = 1^-$ band from the observation of γ ray with

TABLE II. The sequences of states which can belong to rotational bands [from the CHUCK3 fit, the (p,t) cross sections, and the inertial parameters]. More accurate values of energies are taken from the first two columns of Table I.

0^+	1^+	2^+	3^+	4^+	5^+	6^+	7^+	8^+
0.0		47.6		156.6		322.7		541.1
691.4		734.6		833.1		984.9		1186.6
		866.8	911.5	970.7		(1132.7)		
		1132.7		1226.8		1372.0		
or				1226.8		1372.0		
				1194.0		1314.8		
927.3		967.6						
1277.2		1301.4		1361.5		1460.4		
		1489.2		1572.9		1700.5		
1482.2		1520.4		1605.4		1737.4		
1569.0		1600.2		1673.2		1790.8		
		1647.7		1744.4		1880.8		
1797.0		1838.6						
1821.8		1870.9						
1861.0		(1915.2)						
1931.0		1970.7		2068.6				
or								
1931.0		1977.8						
		2059.8		2135.9		2254.4		
		2146.5		2231.3				
		2203.8		2312.2				
		2418.8		2527.2				
		2673.5		2754.3		2878.3		
		2779.1		2889.8		3058.3		
		2791.0		2899.2				
2917.4		2959.7						
	1^-	2^-	3^-	4^-	5^-	6^-	7^-	8^-
	563.2		629.0		746.8		915.2	
		1016.8	1050.9	1098.2	1155.4			
	(1141.5)	1173.06	1211.3		(1321.8)			
			1264.8		1391.7			
			1679.8		1758.9			

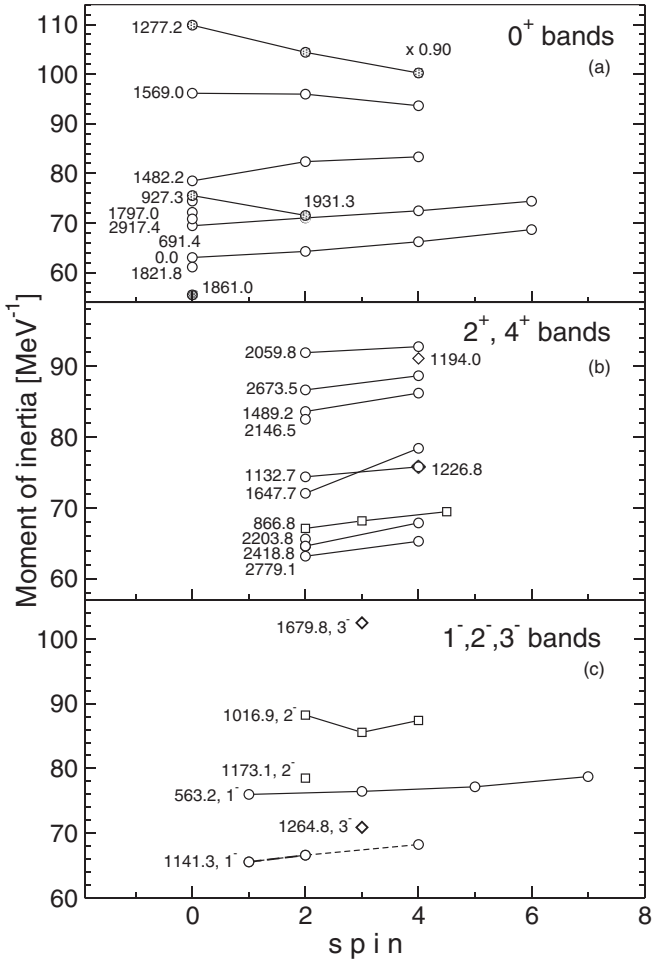

FIG. 8. Moments of inertia for the bands in ^{232}U, as assigned from the angular distributions from the ^{234}U$(p,t)^{232}$U reaction. Values of $J/\hbar^2$ are given. In the graph, they are placed at spins of the first state from the two used in the calculations of every value.

this energy [26]. The corresponding line in the triton spectra is absent. After our firm assignment of spin 4^+ to the state at 1194.1 keV, this proposal has to be rejected because the 1146.3-keV transition should be referred to the decay of this level to the 2^+ level at 47.6 keV. At the same time that a line in the triton spectra is observed at 1141.5 keV, the spin of corresponding state is assigned tentatively as 1^-. Considering this level as the bandhead for the 1^- band with two levels known from previous studies [17], the MoI can be calculated. The procedure described above cannot be applied in this case because of the mixing by the Coriolis interaction. A simplified expression for the band energies can be used in the analysis (for details, see Ref. [11]):

$$E(I,K^\pi = 1^-) \sim E_1 + (A_1 + B)I(I+1) \text{ for } I \text{ odd},$$
$$E(I,K^\pi = 1^-) \sim E_1 + A_1 I(I+1) \text{ for } I \text{ even}. \quad (1)$$

Considering E_1, A_1, and B as parameters, we obtained from the energies of three levels $E_1 = 1127.3$ keV, $A_1 = 7.63$ keV, and $B = -0.47$ keV. This corresponds to a moment of inertia of 65.5 MeV^{-1} (see Fig. 8). The difference to the moment of inertia of the 0^- band is quite large and the energy of 1173.1 keV of the 2^- level of thus assumed 1^- band is much higher than the energy of 1016.8 keV of the 2^- level of the assumed the 2^- band (should be the opposite). If, however, we consider the 1173.1-keV state as the bandhead of the $K^\pi = 2^-$ band, then the moment of inertia is determined as 78.5 MeV^{-1} close to the moment of inertia of the $K^\pi = 0^-$ band. Although some ambiguity remains, the level 3^- at 1264.8 keV can be proposed as the bandhead of the $K^\pi = 3^-$ band.

In a more advanced model [27], which takes into account the Coriolis interaction between all octupole bands, one can fit 11 parameters (bandhead energies, rotation parameters, and Coriolis intrinsic matrix elements between bandheads) to the experimental energies. The former level assignment gives $E_0 = 551.0$ keV, $E_1 = 1136$ keV, $E_2 = 1006$ keV, $E_3 = 1241$ keV, with $\chi^2 = 0.97$, while the latter gives a slightly better value of $\chi^2 = 0.63$ and reasonable values of the fitted energies $E_0 = 551.6$ keV, $E_1 = 987.4$ keV, $E_2 = 1158$ keV, $E_3 = 1240$ keV. However, the predicted 1^- bandhead at 994 keV is not observed experimentally.

The 2^+, 4^+, *and* 6^+ *states.* States with spins and parities firmly assigned as 2^+ excitations dominate in the triton spectra. Some of them are assigned as members of $K^\pi = 0^+$ bands and others probably are bandheads and the levels with spins 4^+ and even 6^+ are identified as possible members of these bands. From the analysis of the γ spectra [17], the 866.8-keV state was identified as the bandhead of the γ-vibrational band with members 911.5 and 970.7 keV. A possible continuation of this band can be the 1132.7-keV state, because for this state the typical 2^+ angular distribution is distorted by a possible admixture of a 6^+ state (it might be a doublet of 2^+ and 6^+ states). The 1132.7-keV state was tentatively identified as the bandhead of the $K^\pi = 2^+$ in Ref. [26] using the analysis of the γ spectra. The 4^+ states at 1226.8 keV and the 6^+ state at 1372.0 keV could be proposed as members of this band. However, the cross section for the 4^+ state exceeds the one for the 2^+ state, contrary to the above conditions. Therefore, the $K^\pi = 4^+$ band is offered as an option.

The 0^+ *states.* For the state at the energy of 927.3 keV assigned in Ref. [25] and in this study as a 0^+ state no members of the band were observed in the (p,t) reaction. The energy 967.6 keV was accepted for the 2^+ member of the band, as suggested in Ref. [25]. The 0^+ state at 1277.2 keV is strongly excited and the members of the assumed band have to be excited too. A clear sequence of states is observed with a spin assignment of 2^+, 4^+, and 6^+, as can be seen in Table II, but MoI determined from this sequence are very high (124 MeV^{-1} from the 2^+ and 0^+ state energy difference) and are decreasing as a function of spin. Other possible sequences do not meet the conditions set forth above. A possible explanation for such a behavior was suggested in Ref. [11], but it is hardly applicable in this case. An assumption may be suggested that the structure of this state is different from those of other collective states. To some extent the same remark can be attributed to the band probably built on the 0^+ state at 1569.0 keV, whose moment of inertia weakly decreases as a function of spin, though weakly. The 0^+ states at 1797.0, 1821.8, and 1861.0 keV are also strongly excited and the excitation of other members of the assumed bands have to be seen in the (p,t) reaction.

At least the 2^+ members can be attributed to such bands built on the 0^+ states at 1797.0 and 1821.8 keV. For the 0^+ state at 1861.0 keV, no prolongation of the band is clearly visible in the triton spectra. Only the unlikely assumption can be made that the corresponding line is hidden under the 1915.2 keV line, but the moment of inertia of 55.4 MeV^{-1} from this assumption is much less than the one for the g.s. An ambiguous situation is met also for the 0^+ state at 1931.0 keV, whose excitation is only slightly weaker than the first excited state at 691.4 keV. Two different sequences may be assumed for the band built on this state, but for both the moment of inertia is decreasing with spin. As it was noted already, the angular distribution for the state at 2917.4 keV differs considerably from all others and can be fitted only by the calculation for transfer of the $(1j_{15/2})^2$ neutron configuration.

Moments of inertia. The MoI of the g.s. of ^{232}U is 63 MeV^{-1}, and as such much higher than in ^{228}Th and ^{230}Th. The $K^\pi = 0^-$ band with the bandhead 1^- at 563.2 keV is well established; it exhibits an MoI increase of about 20% and can serve as orientation for such excitations. The assumption that the 2^- level at 1173.1 keV belongs to the $K^\pi = 1^-$ band is not confirmed by the present analysis (see above). If, however, we assume that the state at 1173.1 keV is the bandhead of the $K^\pi = 2^-$ band, then the MoI determined from the $3^- - 2^-$ energy difference is 78.5 MeV^{-1}, only slightly higher than the MoI of the $K^\pi = 0^-$ band. Although the ambiguity remains, the level 2^- at 1016.9 keV is the member of the $K^\pi = 1^-$ band (with the 1^- level not observed) and the 3^- at level 1264.8 keV can be proposed as the bandhead of the $K^\pi = 3^-$ band.

Unlike in ^{228}Th and ^{230}Th, the MoI of the bands built on the excited 0^+ states in ^{232}U are not much higher than those for the g.s. band. Only two bands, starting at 1227.2 and 1569.0 keV, have a significant excess of the MoI. The principal difference is that the first excited 0^+ state in ^{232}U seems to be a β-vibrational state. The results of the analysis of γ spectra and the MoI value close to the one of the g.s. give evidence for such conclusion. At the same time the first excited 0^+ state in ^{228}Th [11] as well as in ^{240}Pu [3] may have an octupole two-phonon nature. The first excited (possible β-vibrational) state in ^{232}U is most strongly excited, just the same as the the first excited (octupole two-phonon) states in ^{228}Th and ^{240}Pu and the first excited state in ^{230}Th with a more complicated phonon structure [10]. In ^{232}U, the state at 927.3 keV was suggested in Ref. [25] to be an octupole two-phonon excitation. It is confirmed by the large values of the $B(E1)/B(E2)$ ratio calculated using the data on the γ intensities for transitions from 0^+ and 2^+ levels of this band to the levels of the 0^- and g.s. bands [25] (see discussion below and Tables III and V).

The MoI of the 927.3-keV band confirms this assignment, though it is only 16% larger than that of the g.s., compared to a larger excess of 36% and 23% for ^{228}Th and ^{230}Th, respectively. All these facts indicate that the strong population of the first excited 0^+ states does not allow to identify their phonon structure.

The value of the MoI for the band built on the 2^+ state at 866.8 keV is close to the one for the possible β-vibration band (they are only 6% and 8% larger than those of the g.s. band), thus confirming its interpretation as a γ-vibrational band. As for the experimental evidence of the nature of other 0^+ states, we derived only values of the MoI from the sequences of states treated as rotational bands and thus only tentative conclusions can be drawn about their structure. In contrast to ^{230}Th [10], for which they are distributed almost uniformly over the region until 1.80 of the g.s. value (equal to 56 MeV^{-1}) and to ^{228}Th, for which most of values are in the range of 1.35–1.85 of the g.s. value (equal to 52 MeV^{-1}), most of the MoI values of the 0^+ states in ^{232}U do not exceed the value of 1.27 of the g.s. (equal to 63 MeV^{-1}). This fact can indicate that the corresponding states are possibly of quadrupole one-phonon or two-phonon nature.

B. IBM calculations

The interacting boson model (IBM) describes the low-lying positive and negative-parity states by treating the valence nucleons in pairs as bosons. The positive-parity states are described by introducing s and d bosons, which carry angular momentum of $L^\pi = 0^+$ and $L^\pi = 2^+$, respectively, while the negative-parity states can be calculated by additionally including p and f bosons having $L^\pi = 1^-$ and $L^\pi = 3^-$, respectively. In the present paper the IBM-1 version of the model is used, which means that no distinction is made between protons and neutrons [28]. Full IBM-$spdf$ calculations including both sd and pf bosons have been previously done with success in Refs. [29–31].

The octupole degree of freedom is well known for playing a major role in the actinide region [32,33]. In fact, octupole correlations have been predicted to be present in the $Z \sim 88$ and $N \sim 134$ region [34] and have attracted a lot of experimental investigations centered on energy spectra and transition probabilities [35]. The low-lying properties of these nuclei have been interpreted using a series of theoretical models, including the IBM [30,31], which mainly concentrated on the study of electromagnetic decay properties. In the past years, several nuclei in this region were investigated using the (p,t) reaction and the transfer intensities became available also [2,3]. Therefore, several models tried to describe the complete experimental situation [3,11,13].

As presented also in this paper, an increased number of 0^+ excitations have been populated in the previous two-neutron transfer experiments with a rather high intensity [2,3,10,11]. Because some of these states strongly decay to the negative-parity states, it is believed that the quadrupole and octupole degrees of freedom are closely connected to these excitations. In the IBM, such 0^+ states have been interpreted as having a double-octupole character [3,11]. Although this simple picture may not be entirely correct, the IBM has been proved to reasonably describe simultaneously the electromagnetic and transfer properties. To reproduce the experimental features, one has to abandon the description of the nuclei using a simplified Hamiltonian, which is suited to describe mainly electromagnetic data. Such calculations were found to completely fail to reproduce the (p,t) spectroscopic factors by predicting a transfer strength of 1% of that of the g.s., while experimentally the summed transfer intensity amounts to about 80% in this region. The solution seems to be the introduction of the second-order O(5) Casimir operator in the Hamiltonian, which allows for a far better description of the complete experimental data.

In the present work, calculations were performed in the spdf IBM-1 framework using the extended consistent Q formalism (ECQF) [36]. The Hamiltonian employed in the present paper is

$$\hat{H}_{\rm spdf} = \epsilon_d \hat{n}_d + \epsilon_p \hat{n}_p + \epsilon_f \hat{n}_f + \kappa(\hat{Q}_{\rm spdf} \cdot \hat{Q}_{\rm spdf})^{(0)} + a_3[(\hat{d}^\dagger \tilde{d})^{(3)} \times (\hat{d}^\dagger \tilde{d})^{(3)}]^{(0)}, \quad (2)$$

where ϵ_d, ϵ_p, and ϵ_f are the boson energies and $\hat{n}_p$, $\hat{n}_d$, and $\hat{n}_f$ are the boson number operators. In the $spdf$ model, the quadrupole operator is considered as being [37]

$$\hat{Q}_{\rm spdf} = \hat{Q}_{sd} + \hat{Q}_{pf} = (\hat{s}^\dagger \tilde{d} + \hat{d}^\dagger \hat{s})^{(2)} + \chi_{sd}^{(2)}(\hat{d}^\dagger \tilde{d})^{(2)} + \frac{3\sqrt{7}}{5}[(p^\dagger \tilde{f} + f^\dagger \tilde{p})]^{(2)} + \chi_{pf}^{(2)}\left\{\frac{9\sqrt{3}}{10}(p^\dagger \tilde{p})^{(2)} + \frac{3\sqrt{42}}{10}(f^\dagger \tilde{f})^{(2)}\right\}. \quad (3)$$

The quadrupole electromagnetic transition operator is

$$\hat{T}(E2) = e_2 \hat{Q}_{\rm spdf}, \quad (4)$$

where e_2 represents the boson effective charge.

The $E1$ transitions are described in the IBM by a linear combination of the three allowed one-body interactions,

$$\hat{T}(E1) = e_1\big[\chi_{sp}^{(1)}(s^\dagger \tilde{p} + p^\dagger \tilde{s})^{(1)} + (p^\dagger \tilde{d} + d^\dagger \tilde{p})^{(1)} + \chi_{df}^{(1)}(d^\dagger \tilde{f} + f^\dagger \tilde{d})^{(1)}\big], \quad (5)$$

where e_1 is the effective charge for the $E1$ transitions and $\chi_{sp}^{(1)}$ and $\chi_{df}^{(1)}$ are two model parameters.

At this point, one has to introduce an additional term to describe the connection between states with no (pf) content with those having $(pf)^2$ components. This term is very useful to describe both the $E2$ transitions and also the transfer strength between such states. Therefore, the same dipole-dipole interaction term is introduced in the present calculations as previously used in Refs. [11,29,31]:

$$\hat{H}_{\rm int} = \alpha \hat{D}^\dagger_{\rm spdf} \cdot \hat{D}_{\rm spdf} + {\rm H.c.} \quad (6)$$

where

$$\hat{D}_{\rm spdf} = -2\sqrt{2}[p^\dagger \tilde{d} + d^\dagger \tilde{p}]^{(1)} + \sqrt{5}[s^\dagger \tilde{p} + p^\dagger \tilde{s}]^{(1)} + \sqrt{7}[d^\dagger \tilde{f} + f^\dagger \tilde{d}]^{(1)} \quad (7)$$

is the dipole operator arising from the O(4) dynamical symmetry limit, which does not conserve separately the number of positive- and negative-parity bosons [38,39].

The goal of the present paper is to describe simultaneously both the existing electromagnetic and the transfer strength data. To achieve this goal, two-neutron transfer intensities between the g.s. of the target nucleus and the excited states of the residual nucleus were also calculated. The $L = 0$ transfer operator has the following form in the IBM,

$$\hat{P}_\nu^{(0)} = (\alpha_p \hat{n}_p + \alpha_f \hat{n}_f)\hat{s} + \alpha_\nu \left(\Omega_\nu - N_\nu - \frac{N_\nu}{N}\hat{n}_d\right)^{\frac{1}{2}} \left(\frac{N_\nu + 1}{N + 1}\right)^{\frac{1}{2}} \hat{s}, \quad (8)$$

where Ω_ν is the pair degeneracy of the neutron shell, N_ν is the number of neutron pairs, N is the total number of bosons, and α_p, α_f, and α_ν are constant parameters. In this configuration, the $L = 0$ transfer operator contains additional terms besides the leading-order term (third term) [28], which ensures a nonvanishing transfer intensity to the states with $(pf)^2$ configuration.

The calculations were performed using the computer code OCTUPOLE [39] by allowing up to three negative-parity bosons. The following parameters in the Hamiltonian have been used: $\epsilon_d = 0.27$ MeV, $\epsilon_p = 1.14$ MeV, $\epsilon_f = 0.95$ MeV, $\kappa = -13$ keV, and $a_3 = 0.026$ MeV, which ensures a good reproduction of the low-energy states. The interaction strength is given by the α parameter and is chosen to have a very small value, $\alpha = 0.0005$ MeV, similar to Refs. [30,31], which has a very small influence on the level energies.

The most important result of these (p,t) transfer experiments is the fact they reveal a large number of 0^+ states, the presence of such states at higher excitation energies being the subject of intensive theoretical investigations. Therefore, we present in Fig. 9 the full spectrum of experimental excited 0^+ states in comparison with the corresponding calculated values. The IBM predicts the existence of 19 0^+ states up to an excitation energy of 3 MeV in comparison with 13 0^+ states excited in the experiment in the same energy range. The calculated distribution of 0^+ states is very similar to the experimental one up to around 2 MeV. The situation is completely different between 2 and 3 MeV, where a large gap is seen in the experiment up to 2.9 MeV, while the IBM predicts an increased number of states with increasing excitation energy. In the experiment, we can speculate that in this region the 0^+ states carry very small transfer strengths; therefore, the sensitivity of our experiment was not sufficient to discriminate between individual states. Most of the calculated excitations in this energy range are having two pf bosons in their structure (states marked with asterisk), therefore being related to the presence of double dipole-octupole structure [30]. Although it is very interesting that IBM describes both the electromagnetic and the transfer data at the same time, this is most likely not the only mechanism providing an increased number of 0^+ states and therefore we cannot make a definite conclusion on the nature of these excitations based only on these limited experimental data. To support such a claim, more experimental information is needed and, in particular, the $E1$ and $E3$ transition probabilities to the negative-parity states. In Fig. 9, the 2^+ and 4^+ levels revealed in the present experiment are also compared with the predictions of the IBM. The experiment revealed 40 firmly assigned excited 2^+ states and 26 solid assigned excited 4^+ states up to 3.2 MeV. In the same energy range, the calculations produced 26 excited 2^+ states and 26 4^+ excitations.

Because the octupole degree of freedom plays an important role in this mass region, it is crucial for a model to describe at the same time at least the $B(E1)$ and the $B(E1)/B(E2)$ ratios if the reduced transition probabilities have not been measured. In the IBM, the $E1$ transitions are calculated with Eq. (5), while the $E2$ transitions were calculated using Eq. (4). In the present calculations, we have used ($\chi_{sd}^{(2)} = -1.32$,

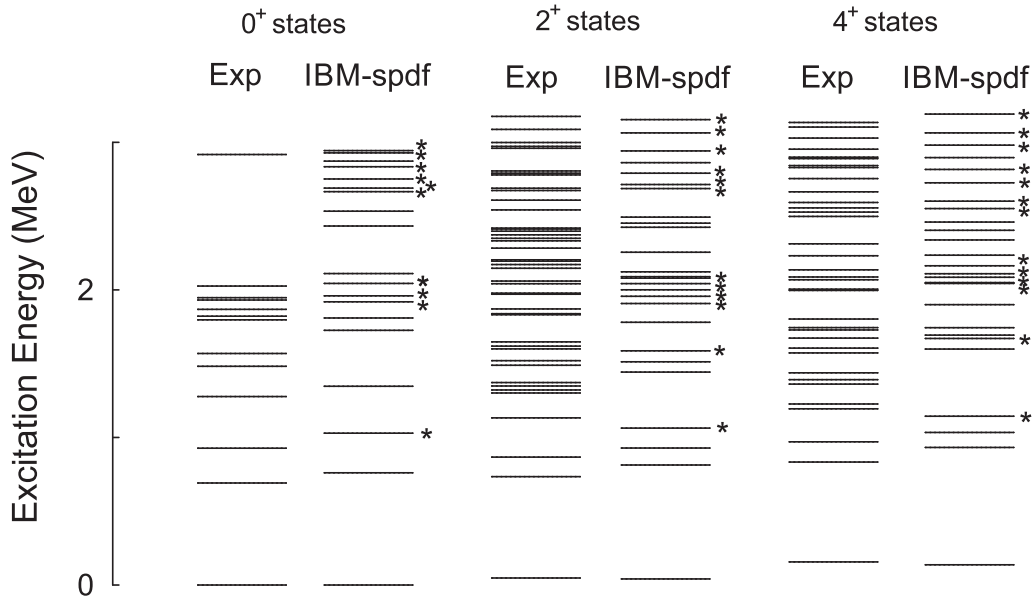

FIG. 9. Energies of all experimentally assigned excited 0^+, 2^+, and 4^+ states in ^{232}U in comparison with IBM-$spdf$ calculations. The states containing two pf bosons in their structure and assumed to have a double dipole-octupole character are marked with an asterisk.

$\chi_{pf}^{(2)} = -1$) as the quadrupole operator parameters and $\chi_{sp} = \chi_{df} = -0.77$ for the parameters in Eq. (5). The remaining parameters are the effective charges and are used to set the scale of the corresponding transitions: $e_1 = 0.0065$ $e$fm and $e_2 = 0.184$ eb.

The $B(E1)/B(E2)$ ratios discussed in Table III belong to the $K^\pi = 0_3^+$ band (the predicted double-octupole phonon band). All the states belonging to this band have $(pf)^2$ bosons in their structure in the IBM calculations and are supposed to have a double-octupole phonon character. The agreement in Table III between experiment and calculations is remarkably good, giving even more confidence in the structure proposed by the IBM. If other excited 0^+ levels decay to the negative-parity states, one would need the crucial information about the decay pattern of these levels. This can be achieved by future $(p,t\gamma)$ and $(n,n'\gamma)$ experiments and we stress here the necessity of performing such delicate investigations.

TABLE III. Experimental and calculated $B(E1)/B(E1)$ (from the 0_1^- state) and $B(E1)/B(E2)$ (from the 0_3^+ state) transition ratios in ^{232}U. The parameters of the $E1$ operator are fitted to the experimental data available. The $B(E1)/B(E2)$ ratios are given in units of 10^{-4} b^{-1}.

K^π	E_i (keV)	J_i	J_{f1}	J_{f2}	Expt.	IBM
0_1^-	563	1^-	2_1^+	0_1^+	1.89(8)	1.89
	629	3^-	4_1^+	2_1^+	1.19(5)	1.17
	747	5^-	6_1^+	4_1^+	0.94(8)	0.97
0_3^+	927	0^+	1_1^-	2_1^+	44(7)	58
	968	2^+	1_1^-	0_1^+	150(30)	122
		2^+	1_1^-	2_1^+	45(1)	85
		2^+	1_1^-	4_1^+	24(1)	47
		2^+	3_1^-	0_1^+	337(68)	167
		2^+	3_1^-	2_1^+	101(3)	117
		2^+	3_1^-	4_1^+	54(1)	65

The experimental integrated two-neutron transfer intensities are displayed in Fig. 10(a). In contrast to ^{228,230}Th, where the spectrum is dominated by a single state with high cross section of about 15%–20% of that of the g.s., the transfer intensity in ^{232}U goes not only to the first excited 0^+ state, but also to a group of states around 2 MeV, which carries more than 30%. In the IBM [Fig. 10(b)], the transfer intensity is also split between the first two excited 0^+ states and a group of 0^+ excitations around 2 MeV. To better compare the agreement with the experimental data, one has to look also at the summed transfer intensity, which is presented in Fig. 10(c) for both the experimental and the calculated values. The main characteristics of the experimental transfer distribution are reproduced, namely the increased population of two groups of 0^+ excitations around 1 and 2 MeV, but IBM fails to give a detailed explanation of the individual states. To perform the IBM calculations, the parameters from Eq. (8) were estimated from the fit of the known two-neutron transfer intensities (integrated cross sections) in Table I. The values employed in the present paper are $\alpha_p = 0.51$ mb/sr, $\alpha_f = -0.45$ mb/sr, and $\alpha_1 = 0.013$ mb/sr.

C. QPM calculations

To obtain a detailed information on the properties of the states excited in the (p,t) reaction, a microscopic approach is necessary. The ability of the QPM to describe multiple 0^+ states (energies, $E2$ and $E0$ strengths, two-nucleon spectroscopic factors) was demonstrated for ^{158}Gd [12]. In a subsequent paper, the QPM was applied to the microscopic structure of 0^+ states in ^{168}Er and three actinide nuclei (^{228}Th, ^{230}Th, and ^{232}U) [13]. Single-particle basis states up to 5 MeV

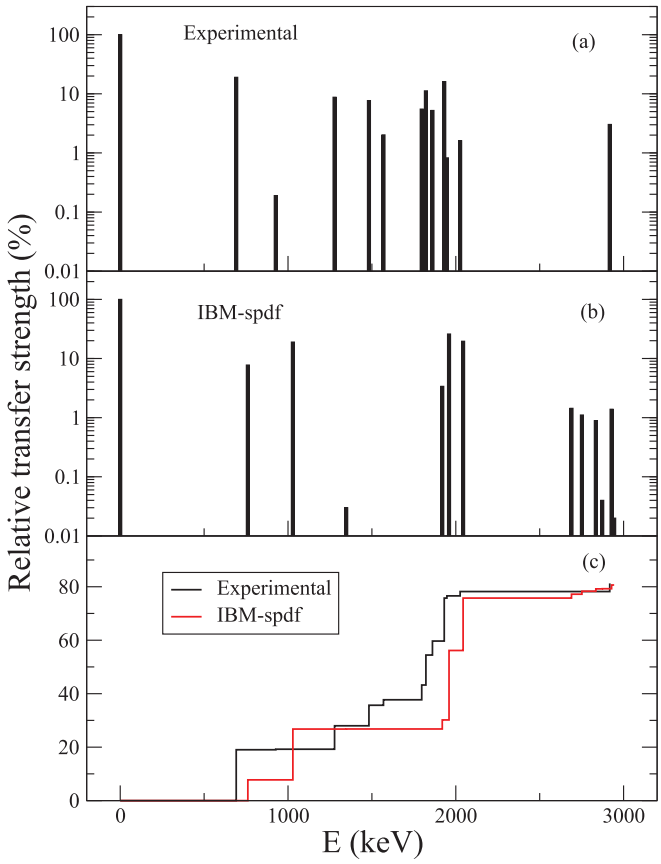

FIG. 10. (Color online) Comparison between the experimental (both firm and tentatively assigned states are included in the figure) two-neutron transfer intensities (a) for the 0^+ states and the IBM predictions (b). In panel (c) the experimental versus computed running sum of the (p,t) strengths is given.

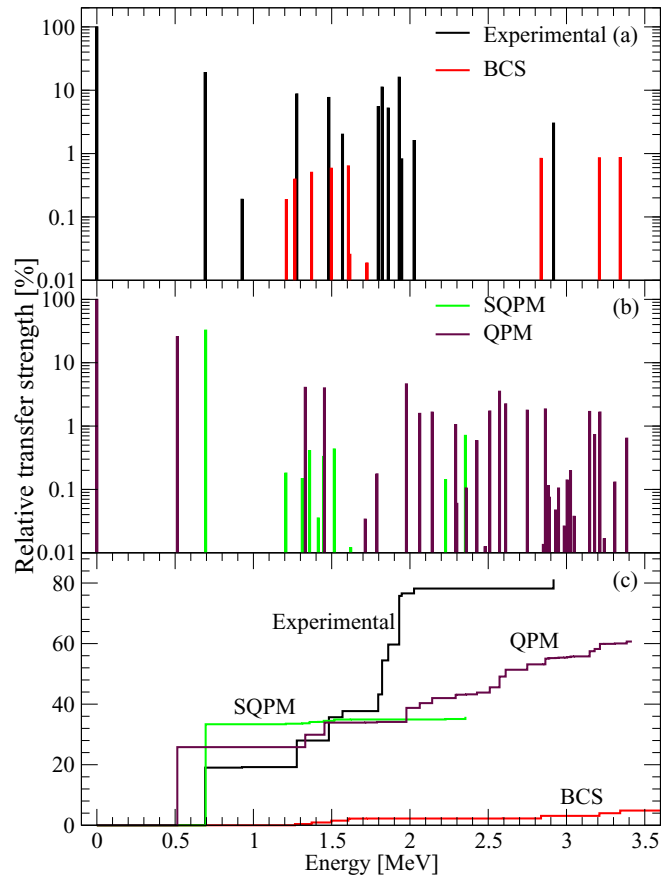

FIG. 11. (Color online) Comparison of experimental and BCS in panel (a), SQPM and QPM in panel (b), 0^+ (p,t) normalized relative strengths. The value for the $0^+_{\text{g.s.}}$ is normalized to 100. The experimental increments of the (p,t) strength in comparison to the QPM, SQPM, and BCS calculations are shown in panel (c).

were generated by a deformed axially symmetric Woods-Saxon potential. Two-body potentials were represented by a monopole plus multipole pairing interaction and isoscalar and isovector multipole-multipole interactions. Two-phonon states were calculated for multipolarities $\lambda = 2$–5. These calculations are also used to compare to the present detailed analysis of the experimental data for ^{232}U. As for the theoretical basis of the calculations, we refer to the publications [13,40].

The (p,t) normalized relative transfer spectroscopic strengths in the QPM are expressed as ratios

$$S_n(p,t) = \left[\frac{\Gamma_n(p,t)}{\Gamma_0(p,t)}\right]^2, \tag{9}$$

where the amplitude $\Gamma_n(p,t)$ includes the transitions between the ^{234}U g.s. and one-quadrupole $K = 0$ phonon components of the ^{232}U wave function. The amplitude $\Gamma_0(p,t)$ refers to the transition between the ^{234}U and ^{232}U g.s. The selected normalization assures that $S_0(p,t) = 100$ for the g.s. transition.

To see the role of the two-phonon and pairing-vibrational excitations in the QPM calculations, we performed a simple QPM (SQPM) calculation using the Nilsson potential plus monopole pairing interaction (Nilsson parameters κ and μ taken from Ref. [27], deformation parameters $\epsilon_2 = 0.192$, $\epsilon_4 = -0.008$ and pairing gaps $\Delta_p = 0.706$ MeV, $\Delta_n = 0.602$ MeV for ^{232}U and $\epsilon_2 = 0.200$, $\epsilon_4 = -0.073$ and pairing gaps $\Delta_p = 0.738$ MeV, $\Delta_n = 0.582$ MeV for ^{234}U from Refs. [41,42]) plus isoscalar and isovector quadrupole-quadrupole and octupole-octupole interactions. Only one-phonon random-phase approximation (RPA) states were taken into account in these calculations. Energies of two-quasiparticle 0^+ states were estimated from the BCS theory. The model predicts 15 neutron two-quasiparticle states of the structure $\alpha^\dagger_q\alpha^\dagger_{\bar{q}}$ below 4 MeV that correspond to broken neutron pairs sensitive to two-neutron transfer. The energies and normalized relative transfer strengths are shown in Fig. 11(a) for $S_n(p,t) \geqslant 0.01$ and compared to the experimental energies and relative transfer strengths. It is evident that the two-quasiparticle 0^+ states represent only a minor contribution to the total relative transfer strength [cf. Fig. 11(c)].

The strengths of the isoscalar and isovector quadrupole-quadrupole interactions in the SQPM, $\kappa^{(0)}_{20}$ and $\kappa^{(1)}_{20}$, respectively, were varied to fit the experimental energies and (p,t) spectroscopic strengths of the lowest 0^+ states. It was found that an effect of $\kappa^{(1)}_{20}$ on the (p,t) spectroscopic strengths is

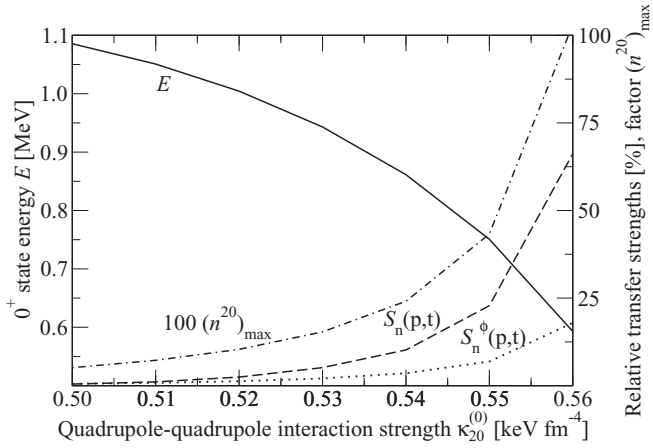

FIG. 12. The SQPM energy E (solid line), the normalized relative transfer strength $S_n(p,t)$ (dashed line), the contribution $S_n^{\phi}(p,t)$ of the backward RPA amplitude ϕ to $S_n(p,t)$ (dotted line), and the maximum number of quasiparticles with quantum number q in the g.s. $(n^{20})_{max}$ (dash-dotted line) as functions of the isoscalar quadrupole-quadrupole interaction strength $\kappa_{20}^{(0)}$ for the first excited 0^+ state, $\kappa_{20}^{(1)} = 0$.

negligible and that $\kappa_{20}^{(0)}$ significantly influences only energy and spectroscopic strength of the first 0^+ excited state. It is known that in the even-even actinides the phonon coupling does not spoil the coherence of pairing correlations in the lowest 0^+ excited state [13]. As a consequence, the state has a pronounced pairing-vibrational character that manifests itself by large RPA backward ϕ amplitudes. From Fig. 12 one can see that the contribution $S_n^{\phi}(p,t)$ of the backward RPA amplitudes to the normalized relative transfer spectroscopic strength $S_n(p,t)$ is important for the first excited 0^+ state, thus indicating its pairing-vibrational character. The pairing interaction is essential for reproducing the experimental relative transfer strength of the first excited 0^+ state. If we artificially lower the neutron and proton pairing interaction strengths and simultaneously change the isoscalar quadrupole-quadrupole interaction strength to fit the experimental energy of the first excited 0^+ state, both $S_n^{\phi}(p,t)$ and $S_n(p,t)$ rapidly drop down. The SQPM predicts $B(E2) = 4$ W.u. for the transition from the first excited 0^+ state to the 2^+ member of the g.s. band, the QPM gives a slightly lower value of 2.3 W.u. Therefore, we can assume that the lowest 0^+ excited state (0_2^+) has a mixed pairing-vibrational and β-vibrational character. The contribution of $S_n^{\phi}(p,t)$ for higher excited 0^+ states in the SQPM is significantly lower and in most cases negligible, thus indicating their weak phonon-vibrational or two-quasiparticle character. The maximum value of the number of quasiparticles with the quantum number q in the g.s., n_{max}^{20}, measures the g.s. correlations and can be calculated from (see Ref. [43])

$$n_{max}^{20} = \max\left[\tfrac{1}{2}\left(\phi_{qq}^{20}\right)^2\right], \tag{10}$$

where ϕ_{qq}^{20} are the backward RPA amplitudes of the first 0^+ excited state. For the isoscalar quadrupole-quadrupole interaction strength $\kappa_{20}^{(0)} = 0.554$ keV fm^{-4}, which reproduces the experimental energy of the first 0^+ excited state, the g.s. correlations estimated by n_{max}^{20} become large (see Fig. 12). As a consequence, the RPA approximation used in the SQPM is no more accurate and multiphonon admixtures and interactions between phonons have to be taken into account.

TABLE IV. Phonon structure of the QPM 0^+ states up to 2.6 MeV [44]. The weights of the one-phonon $(\lambda\mu)_i$ or the two-phonon $[(\lambda\mu)_i(\lambda\mu)_i]$ components are given in percent. Only main one-phonon and two-phonon components are shown. Transfer factors $S(p,t)$ are normalized to 100 for the $0^+_{g.s.}$.

K_n^{π}	E_n (calc.)	$S(p,t)_{calc.}$	Structure
0_2^+	0.51	25.81	$(20)_1 91$
0_3^+	1.33	4.09	$(20)_2 90; [(22)_1(22)_1]4$
0_4^+	1.45	4.01	$(20)_3 27; (20)_5 27; [(22)_1(22)_1]19; [(30)_1(30)_1]2$
0_5^+	1.71	0.03	$(20)_3 57; (20)_5 23; (20)_4 12$
0_6^+	1.79	0.18	$(20)_4 79; [(22)_1(22)_1]3$
0_7^+	1.98	4.64	$(20)_5 15; (20)_7 15; (20)_9 13; [(22)_1(22)_1]16; [(30)_1(30)_1]4$
0_8^+	2.06	1.59	$(20)_6 90$
0_9^+	2.14	1.67	$(20)_7 55; (20)_5 11; [(31)_1(31)_1]3; [(32)_1(32)_1]3$
0_{10}^+	2.29	1.06	$(20)_9 49; (20)_7 14; [(32)_1(32)_1]11$
0_{11}^+	2.30	0.06	$(20)_9 4; [(44)_1(44)_1]92$
0_{12}^+	2.36	0.11	$(20)_8 65; (20)_{12} 16; [(30)_1(30)_1]2$
0_{13}^+	2.43	0.59	$(20)_{10} 7; [(32)_1(32)_1]65$
0_{14}^+	2.48	0.01	$(20)_{10} 63; (20)_9 11; [(32)_1(32)_1]8$
0_{15}^+	2.51	1.73	$(20)_{11} 43; [(30)_1(30)_1]37$
0_{16}^+	2.57	3.55	$(20)_{11} 43; [(30)_1(30)_1]29$

In Figs. 11(a) and 11(b) the experimental spectrum of the 0^+ (p,t) normalized relative transfer strengths is compared to the results of the SQPM and QPM calculations. The numerical results of the QPM calculations from Ref. [13] are provided to us by Sushkov [44]. Both SQPM and QPM calculations reproduce the strong excitation of the first 0^+ excited state in accordance with the experiment. The SQPM generates 9 0^+ states below 2 MeV, in fair agreement with the 10 firmly assigned states and 3 0^+ states in the region 2–3 MeV compared to 2 experimentally assigned states. The QPM fails to reproduce the experimental number of the 0^+ states. It predicts only 6 0^+ states below 2 MeV and 20 0^+ states in the region 2–3 MeV. The difference in the number of the 0^+ states between the SQPM and the QPM is caused mainly by the truncated SQPM model space (two-phonon states not considered).

In Fig. 11(c) we present also the increments of the experimental relative transfer strength in comparison to those of the BCS, SQPM, and QPM. Additional interactions in the QPM lead to level repulsion (excited 0^+ states spectrum broadening) and transfer strength fragmentation (lower relative transfer strength for the first excited 0^+ state in favor of higher excited states up to 2 MeV). In the region above 1.8 MeV, both SQPM and QPM fail to reproduce the sharp experimental increase of the (p,t) strength running sum. In Table IV, structure and

TABLE V. Experimental and SQPM $B(E1)/B(E2)$ transition ratios in ^{232}U between the states of the 0_3^+ band and the 0_1^- and 0_1^+ bands in units of 10^{-4} b^{-1}.

K_i^π	J_i	J_{f1}	J_{f2}	Expt.	SQPM
0_3^+	0^+	1_1^-	2_1^+	44(7)	7.5
	2^+	1_1^-	0_1^+	150(30)	15
	2^+	1_1^-	2_1^+	45(1)	11
	2^+	1_1^-	4_1^+	24(1)	5.8
	2^+	3_1^-	0_1^+	337(68)	23
	2^+	3_1^-	2_1^+	101(3)	16
	2^+	3_1^-	4_1^+	54(1)	8.8

normalized relative transfer strength of the QPM 0^+ excited states are presented. It is difficult to make an assignment to experimental levels above 1.5 MeV. The second two excited states, 0_3^+ and 0_4^+, most probably correspond to the experimental levels at 1.277 and 1.482 MeV, which is supported by the similarly normalized relative transfer strengths. The experimental level at 0.927 MeV with the high $B(E1)/B(E2)$ transition ratios and low normalized relative transfer strength is not reproduced, neither in the SQPM (see Table V) nor in the QPM [13]. Contrary to the IBM, two-octupole phonon states are shifted to higher energies ~2.4–2.5 MeV owing to the Pauli exclusion principle. The lower-lying states (e.g., 0_4^+ at 1.45 MeV) possess only small two-octupole phonon admixtures. However, for the octupole-octupole isoscalar strength $\kappa_{30}^{(0)} = 7$ eV fm^{-6}, which reproduces the experimental energy of the first 1^- excited state, the SQPM predicts enhanced $E1$ transitions from the $K = 0^-$ band to the g.s. band, e.g., $B(E1; 1_1^- \rightarrow 0_1^+) = 0.2\ e^2$ fm$^2 = 0.08$ W.u. As a consequence, even a small admixture of double-octupole phonon configuration $[(30)_1(30)_1]$ in 0_3^+ of about 0.3%–0.6% can account for the experimentally observed $B(E1)/B(E2)$ ratios (see Table V).

The SQPM and the QPM are quite accurate in nuclei with small g.s. correlations. Because in ^{232}U the g.s. correlations (as tested for the SQPM) become large, the effect of multiphonon admixtures (three and more phonons) in the QPM that pushes two-phonon poles and consequently two-phonon energies to lower values is then underestimated. In future QPM studies one also has to take into account the spin-quadrupole interaction that is known to influence the density and structure of low-lying 0^+ states [45].

D. To the density distribution of excited 0^+ states

As one can see in Fig. 7, 0^+ states are observed in a limited area in the form of a bump. Local groups of 2^+, 4^+, and 6^+ states are shifted relative to 0^+ states in the direction of higher energies. The assumption that the 0^+ states are localized mainly in a limited region and that the density of the 0^+ levels above 3 MeV is, at least, negligible was made in Ref. [10]. With this purpose, the triton spectra from the ^{232}Th$(p,t)^{230}$Th reaction were measured for the energy range of 3–4 MeV, but only for the angles 12.5° and 26°. Two lines in the spectra meet the condition not only for the 0^+ state, but also for 6^+

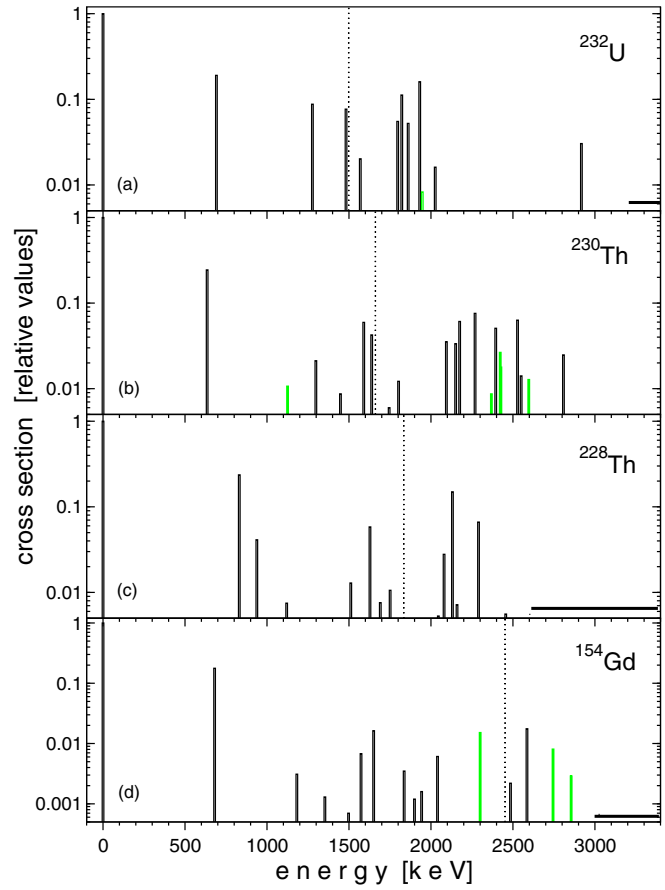

FIG. 13. (Color online) Location and the (p,t) strength of 0^+ states in ^{232}U, ^{230}Th, ^{228}Th, and ^{154}Gd. The dotted lines indicate the pairing gap for each nucleus. Horizontal lines indicate limitations in the investigation energy.

states. Figure 13 shows the 0^+ state spectra of studied actinides and as an example one of the rare-earth nucleus, ^{154}Gd. In the rare-earth region, spin-parity values 0^+ were assigned for many nuclei using the triton angular distributions for only three [5,8] and even two [9] angles, exploring the fact that the $L = 0$ transfer angular distribution peaks strongly at forward angles. As one could see, some of the $L = 2$ and 4 angular distributions also peak strongly at forward angles. Therefore, some tentative assignments of spin 0^+ just below 3 MeV (as for ^{154}Gd) do not actually belong to the 0^+ states. Only a detailed fitting of the angular distribution in a sufficiently large range of angles would make it possible to distinguish between the 0^+ and 2^+ or 4^+ assignments.

At the same time, the IBM and the QPM predict an increase in the number of 0^+ states with increasing energy. The impact of the inclusion of these additional levels can be seen from the statistical analysis of the level density for actinides, experimental in the energy interval of 0–3 MeV and predicted by the QPM in the energy interval of 0–4 MeV (Fig. 14). The Brody distribution was used for fitting the normalized nearest-neighbor spacing as a function of a dimensionless spacing variable s [46]. It was applied in Ref. [5]

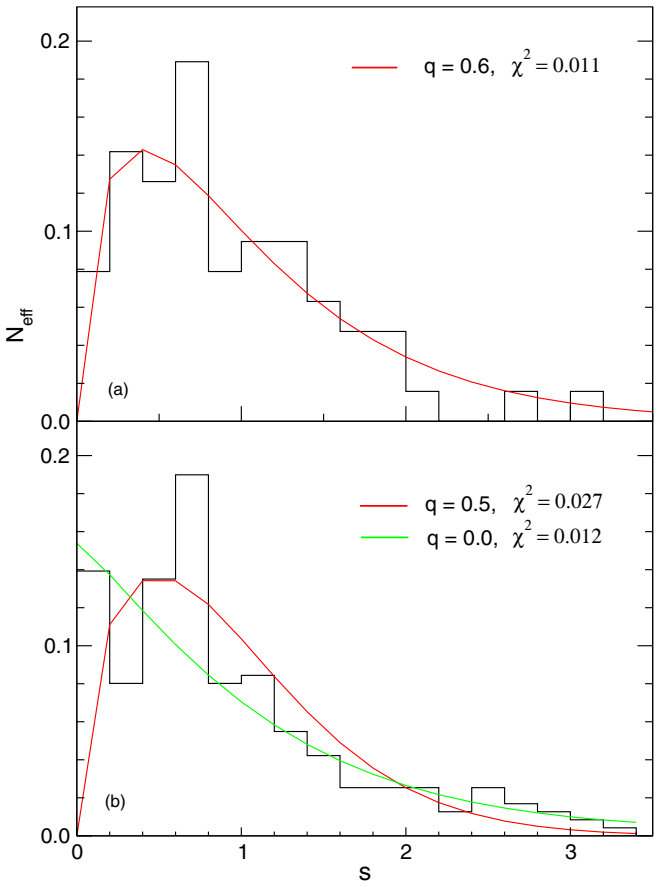

FIG. 14. (Color online) Normalized nearest-neighbor spacing as a function of a dimensionless spacing variable s and fit with the Brody distribution: (a) experimental data for ^{228,230}Th, ^{232}U, and ^{240}Pu in the energy interval of 0–3 MeV, (b) calculated by the QPM data for ^{228,230}Th and ^{232}U in the energy interval of 0–4 MeV.

for analysis of the 0^+ spectra in the rare-earth nuclei testing for the ordered or chaotic (mixed) nature of these spectra. The Brody distribution describes systems with intermediate degrees of mixing depending on the parameter q, which ranges from 0 for a Poisson distribution (ordered nature) to 1 for a Wigner distribution (chaotic nature)

$$N_{\text{eff}} = As^q \exp(-bs^{q+1}), \tag{11}$$

where the parameters b and A are determined by the value of q: $b = \{\Gamma[(2+q)/(1+q)]\}^{q+1}$ and $A = b(1+q)$. To get the value of χ^2, parameter A was left free. In such a way, the experimental data for ^{228,230}Th [10,11], ^{232}U, and ^{240}Pu [3] are fitted by the Brody distribution for $q = 0.6$ (the same as for the rare-earth nuclei in [5]) with $\chi^2 = 0.011$. The theoretical data from Refs. [12,44] can be fitted by the Brody distribution for $q = 0.5$, but only with a worse $\chi^2 = 0.027$. In both cases, the obtained values of the parameter A are close to $A = b(1+q)$. A much better fit is obtained for the Poisson distribution with $\chi^2 = 0.012$. This means that the experimental 0^+ spectrum in the energy interval 0–3 MeV is intermediate between an ordered and a chaotic nature, while the ordered nature is preferred for the theoretical spectrum in the energy interval 0–4 MeV. Besides that, the mean number of 0^+ states observed in one nucleus in the energy range of 0–3 MeV is about 18, while the number of theoretically predicted 0^+ states in the energy range of 0–4 MeV is about 80. Therefore, it is important to investigate at least the region 3–4 MeV for the presence of additional 0^+ excitations.

The phenomenologic IBM-1 used in the present paper even in its simplified two-parametric form is known for its capability to study chaos and transitions between order and chaos in the properties of low-lying collective states of even-even nuclei [47,48]. In the microscopic QPM, an introduction of multiphonon states (three and more) seems to be necessary to move from order towards chaos. This idea is supported by the analysis performed for odd nuclei [49,50], where the addition of one-quasiparticle plus two-phonon states (i.e., "5-qp states") to the standard one-quasiparticle and one-quasiparticle plus one-phonon states led to a fit of the calculated $17/2^+$ ^{209}Pb spectra to the Brody distribution with the parameter $q = 0.6$, thus corresponding to a transitional region between order and chaos.

IV. CONCLUSION

To summarize, in a high-resolution experiment, the excited states of ^{232}U have been studied in the (p,t) transfer reaction. One hundred sixty-two levels were assigned, using a DWBA fit procedure. Among them, 13 excited 0^+ states have been found in this nucleus up to an energy of 3.2 MeV; most of them have not been experimentally observed before. Their accumulated strength makes up 84% of the g.s. strength. Firm assignments have been made for most of the 2^+ and 4^+ states and for about half of the 6^+ states. These assignments made it possible to identify the sequences of states, which have the features of rotational bands with definite inertial parameters. Moments of inertia are derived from these sequences. Most of the values of the MoI are not much higher than the value for the g.s. band. This indicates that they may correspond mainly to a quadrupolar one-phonon structure of 0^+ states.

The experimental data have been compared to IBM-*spdf* and QPM calculations. The IBM reproduces the main characteristics of the experimental transfer distribution, namely the running sum of the (p,t) strengths and increased population of two groups of 0^+ excitations around 1 and 2 MeV, but the strength of the first excited 0^+ state is underestimated and the strength of the second 0^+ state is overestimated. Most of the calculated excitations have two pf bosons in their structure, therefore being related to the presence of a double-octupole structure. Good agreement with experiment for the $B(E1)/B(E2)$ transition ratios indicates also the importance of the octupole degree of freedom. The QPM reproduces the strong (p,t) strength of the first excited 0^+ state owing to its predicted pairing-vibrational character and lower (p,t) strengths for higher-lying 0^+ states. It fails to account for a rapid increase of the running sum of the (p,t) strength above 1.8 MeV and predicts only minor double-octupole phonon components in states below 2.4 MeV. Both models fail to give a detailed explanation of the individual states.

The comparison of the experimental nearest-neighbor spacing distribution of the 0^+ states in the region of 0–3 MeV

for four actinide isotopes (^{228,230}Th, ^{232}U, and ^{240}Pu) to the Brody distribution revealed an intermediate character of the experimental 0^+ spectrum between order and chaos. A similar distribution for the data obtained from the QPM calculations in the region of 0–4 MeV somewhat differs from the experimental one and is closer to the ordered nature. Though the increased role of multiphonon states in the model at higher energies means movement to chaos. Therefore, (p,t) and $(p,t\gamma)$ experiments for higher energies could provide additional information on the nature of 0^+ excitations.

ACKNOWLEDGMENTS

The work was supported by the DFG (Grants No. C4-Gr894/2-3 and No. Zl510/4-2); by the National Programme for Sustainability I (2013–2020) by the state budget of the Czech Republic, Identification Code LO1406; by the Romanian Executive Unit for Financing Higher Education, Research, Development and Innovation under Contracts No. 127/F4 and No. PN-II-ID-PCE-2011-3-0367.

[1] A. I. Levon, J. de Boer, G. Graw, R. Hertenberger, D. Hofer, J. Kvasil, A. Lösch, E. Müller-Zanotti, M. Würkner, H. Baltzer, V. Grafen, and C. Günther, Nucl. Phys. A **576**, 267 (1994).
[2] H.-F. Wirth, G. Graw, S. Christen, D. Cutoiu, Y. Eisermann, C. Günther, R. Hertenberger, J. Jolie, A. I. Levon, O. Möller, G. Thiamova, P. Thirolf, D. Tonev, and N. V. Zamfir, Phys. Rev. C **69**, 044310 (2004).
[3] M. Spieker, D. Bucurescu, J. Endres, T. Faestermann, R. Hertenberger, S. Pascu, S. Skalacki, S. Weber, H.-F. Wirth, N. V. Zamfir, and A. Zilges, Phys. Rev. C **88**, 041303(R) (2013).
[4] S. R. Lesher, A. Aprahamian, L. Trache, A. Oros-Peusquens, S. Deyliz, A. Gollwitzer, R. Hertenberger, B. D. Valnion, and G. Graw, Phys. Rev. C **66**, 051305(R) (2002).
[5] D. A. Meyer, V. Wood, R. F. Casten, C. R. Fitzpatrick, G. Graw, D. Bucurescu, J. Jolie, P. von Brentano, R. Hertenberger, H.-F. Wirth, N. Braun, T. Faestermann, S. Heinze, J. L. Jerke, R. Krücken, M. Mahgoub, O. Möller, D. Mücher, and C. Scholl, Phys. Rev. C **74**, 044309 (2006).
[6] D. Bucurescu, G. Graw, R. Hertenberger, H.-F. Wirth, N. Lo Iudice, A. V. Sushkov, N. Yu. Shirikova, Y. Sun, T. Faestermann, R. Krücken, M. Mahgoub, J. Jolie, P. von Brentano, N. Braun, S. Heinze, O. Möller, D. Mücher, C. Scholl, R. F. Casten, and D. A. Meyer, Phys. Rev. C **73**, 064309 (2006).
[7] L. Bettermann, S. Heinze, J. Jolie, D. Mücher, O. Möller, C. Scholl, R. F. Casten, D. A. Meyer, G. Graw, R. Hertenberger, H.-F. Wirth, and D. Bucurescu, Phys. Rev. C **80**, 044333 (2009).
[8] G. Ilie, R. F. Casten, P. von Brentano, D. Bucurescu, T. Faestermann, G. Graw, S. Heinze, R. Hertenberger, J. Jolie, R. Krücken, D. A. Meyer, D. Mücher, C. Scholl, V. Werner, R. Winkler, and H.-F. Wirth, Phys. Rev. C **82**, 024303 (2010).
[9] C. Bernards, R. F. Casten, V. Werner, P. von Brentano, D. Bucurescu, G. Graw, S. Heinze, R. Hertenberger, J. Jolie, S. Lalkovski, D. A. Meyer, D. Mücher, P. Pejovic, C. Scholl, and H.-F. Wirth, Phys. Rev. C **87**, 024318 (2013).
[10] A. I. Levon, G. Graw, Y. Eisermann, R. Hertenberger, J. Jolie, N. Yu. Shirikova, A. E. Stuchbery, A. V. Sushkov, P. G. Thirolf, H.-F. Wirth, and N. V. Zamfir, Phys. Rev. C **79**, 014318 (2009).
[11] A. I. Levon, G. Graw, R. Hertenberger, S. Pascu, P. G. Thirolf, H.-F. Wirth, and P. Alexa, Phys. Rev. C **88**, 014310 (2013).
[12] N. Lo Iudice, A. V. Sushkov, and N. Yu. Shirikova, Phys. Rev. C **70**, 064316 (2004).
[13] N. Lo Iudice, A. V. Sushkov, and N. Yu. Shirikova, Phys. Rev. C **72**, 034303 (2005).
[14] N. V. Zamfir, Jing-ye Zhang, and R. F. Casten, Phys. Rev. C **66**, 057303 (2002).
[15] Y. Sun, A. Aprahamian, J.-y. Zhang, and C.-T. Lee, Phys. Rev. C **68**, 061301(R) (2003).
[16] R. K. Sheline and P. Alexa, Acta Phys. Pol. B **39**, 711 (2008).
[17] E. Browne, Nucl. Data Sheets **107**, 2579 (2006).
[18] E. Zanotti, M. Bisenberger, R. Hertenberger, H. Kader, and G. Graw, Nucl. Instrum. Methods A **310**, 706 (1991).
[19] H.-F. Wirth, Ph.D. thesis, Technische Universität München, 2001, http://tumb1.biblio.tu-muenchen.de/publ/diss/ph/2001/wirth.html
[20] F. Riess, Beschleunigerlaboratorium München, Annual Report, 1991, p. 168.
[21] F. D. Becchetti and G. W. Greenlees, Phys. Rev. **182**, 1190 (1969).
[22] E. R. Flynn, D. D. Amstrong, J. G. Beery, and A. G. Blair, Phys. Rev. **182**, 1113 (1969).
[23] F. D. Becchetti and G. W. Greenlees, *Proceedings of the Third International Symposium on Polarization Phenomena in Nuclear Reactions, Medison (1970)*, edited by H. H. Barshall and W. Haeberli (University of Wisconsin Press, Medison, 1971), p. 68.
[24] P. D. Kunz, computer code CHUCK3, University of Colorado (unpublished).
[25] G. Ardisson, M. Hussonnois, J. F. LeDu, D. Trubert, and C. M. Lederer, Phys. Rev. C **49**, 2963 (1994).
[26] R. Weiss-Reuter, H. Münzel, and G. Pfennig, Phys. Rev. C **6**, 1425 (1972).
[27] V. G. Soloviev, *Theory of Complex Nuclei* (Pergamon Press, Oxford, UK, 1976).
[28] F. Iachello and A. Arima, *The Interacting Boson Model* (Cambridge University Press, Cambridge, UK, 1987).
[29] J. Engel and F. Iachello, Nucl. Phys. A **472**, 61 (1987).
[30] N. V. Zamfir and D. Kusnezov, Phys. Rev. C **63**, 054306 (2001).
[31] N. V. Zamfir and D. Kusnezov, Phys. Rev. C **67**, 014305 (2003).
[32] L. M. Robledo and R. R. Rodriguez-Guzman, J. Phys. G: Nucl. Part. Phys. **39**, 105103 (2012).
[33] L. M. Robledo and P. A. Butler, Phys. Rev. C **88**, 051302 (2013).
[34] W. Nazarewicz, P. Olanders, I. Ragnarsson, J. Dudek, G. A. Leander, P. Moller, and E. Ruchowska, Nucl. Phys. A **429**, 269 (1984).
[35] P. A. Butler and W. Nazarewicz, Rev. Mod. Phys. **68**, 349 (1996).
[36] R. F. Casten and D. D. Warner, Rev. Mod. Phys. **60**, 389 (1988).
[37] D. Kusnezov, J. Phys. A **23**, 5673 (1990).
[38] D. Kusnezov, J. Phys. A **22**, 4271 (1989).
[39] D. Kusnezov, computer code OCTUPOLE (unpublished).

[40] V. G. Soloviev, *Theory of Atomic Nuclei: Quasiparticles and Phonons* (Institute of Physics, Bristol, UK, 1992).
[41] P. Møller, J. R. Nix, W. D. Myers, and W. J. Swiatecki, At. Data Nucl. Data Tables **59**, 185 (1995).
[42] P. Møller, J. R. Nix, and K.-L. Kratz, At. Data Nucl. Data Tables **66**, 131 (1997).
[43] T. Weber, J. de Boer, K. Freitag, J. Gröger, C. Günther, P. Herzog, V. G. Soloviev, A. V. Sushkov, and N. Yu. Shirikova, Eur. Phys. J. A **3**, 25 (1998).
[44] A. V. Sushkov (private communication).
[45] N. I. Pyatov, Ark. Phys. **36**, 667 (1967).
[46] T. A. Brody, Lett. Nuovo Cimento **7**, 482 (1973).
[47] Y. Alhassid, A. Novoselsky, and N. Whelan, Phys. Rev. Lett. **65**, 2971 (1990).
[48] P. Cejnar and J. Jolie, Prog. Part. Nucl. Phys. **62**, 210 (2009).
[49] Ch. Stoyanov and V. Zelevinsky, Phys. Rev. C **70**, 014302 (2004).
[50] Ch. Stoyanov, Rom. J. Phys. **58**, 1096 (2013).